for the calcium-binding proteins calbindin and calretinin, which shows three strongly labeled horizontal strata of processes (Fig. 3N; Haverkamp and Wässle, 2000; Wässle, 2004). Since the three Wfs1-immunoreactive strata in the IPL corresponded to those immunoreactive for the calcium-binding proteins (Fig. 3M–O), Wfs1 can be used as a marker for the three strongly labeled horizontal strata. In addition, the three strata contain Wfs1-immunoreactive processes of calbindin-D-28K-labeled amacrine and ganglion cells (Fig. 3M–O), since calbindin-D-28K is a marker for both amacrine and ganglion cells (Haverkamp and Wässle, 2000). Of these strata, the inner and outer strata also contain Wfs1-immunoreactive processes of cholinergic amacrine cells, since the two strata were immunoreactive for ChAT (Fig. 3J–L; Haverkamp and Wässle, 2000).

According to a review by Wässle (2004), the outer stratum contains the processes of the OFF-cholinergic amacrine cells, the dendrites of OFF-alpha cells, and the outer dendritic branches of direction selective cells. This band is densely packed with synapses and $GABA_A$ receptors (Brandstätter et al., 1995), and is where transient light responses and OFF direction-selective responses are calculated (Roska and Werblin, 2001). The intermediate stratum separates the OFF sublamina (outer) from the ON sublamina (inner). The polyaxonal amacrine cells (Ölveczky et al., 2003) ramify in this band, as do two GABA-containing amacrine cells. These cells contain, as well as GABA, a neuromodulator (nitric oxide and a catecholamine, respectively). Their functions are unknown. The inner stratum contains the axon terminals of an ON bipolar cell (Brown and Masland, 1999), the processes of the ON-cholinergic amacrine cells, the dendrites of ON-alpha cells, and the inner dendritic branches of direction-selective cells. This stratum is also densely packed with synapses and $GABA_A$ receptors, providing the circuitry for ON-transient light responses and ON direction-selective responses (Wässle, 2004). Thus, it is speculated that the inner stratum contains Wfs1-immunoreactive processes of bipolar cells, as well as those of amacrine and ganglion cells.

***Müller cells.*** Wfs1 protein was expressed strongly in endfeet of Müller cells, moderately in internal radial processes, and weakly in cell bodies, whereas *Wfs1* mRNA signals were weak in the middle row of the INL where cell bodies of Müller cells are located. These results suggest that the turnover of Wfs1 protein in Müller cells is slower than that in other Wfs1-positive retinal neurons. As described above, Wfs1 protein was distributed densely in the endfeet of Müller cells, but sparsely in cell bodies. This evidence indicates that Wfs1 protein accumulates in the endfeet of Müller cells. Elucidating the cause of this accumulation might provide a clue as to the biochemical function of Wfs1 in glial cells including Müller cells.

Although Wolfram syndrome patients often develop diabetes mellitus early on (median age 6 years, range 3 weeks to 16 years; Barrett et al., 1997), they rarely develop diabetic retinopathy (Mtanda et al., 1986; Bitoun, 1994; Seynaeve et al., 1994; Barrett et al., 1997). Diabetic retinopathy is accompanied by a proliferation of new retinal vessels under hypoxic conditions. The proliferation is mediated by Müller cells via the release of vascular endothelial growth factor (VEGF) and transforming growth factor β or via direct contact with endothelial cells (Bringmann and Reichenbach, 2001). In Wolfram syndrome patients it is suggested that the functions of Müller cells are disrupted by loss-of-function mutations in the *WFS1* gene. Thus, the proliferation of new retinal vessels might be hampered by dysfunctional Müller cells in Wolfram syndrome patients.

## Optic nerve

Mice lack intraretinal myelination and a well-developed lamina cribrosa but exhibit a marked concentration of astrocytic filaments at the retinal optic nerve junction (Morcos and Chan-Ling, 2000). Based on this evidence, we divided the mouse optic nerve into three parts (i, afd, and afs) defined by the position of the sensory retina and by the distribution of astrocytic filaments. These criteria for the optic nerve subdivisions are appropriate since the distribution of GS-positive cells corresponded to the afs part. Thus, mouse optic nerve is also divided into three parts by the position of the sensory retina and by the distribution of GS-positive cells as shown in Figure 8Q.

Wfs1-positive astrocytes were distributed in the optic nerve, but not in the retina, optic chiasm, or optic tract (Figs. 8A–I, 10C,D). This evidence suggests that the astrocytes in the optic nerve are different from those in the retina, optic chiasm, and optic tract. Further studies are required to clarify the morphological and functional differences between Wfs1-positive astrocytes in the optic nerve and Wfs1-negative astrocytes in the optic chiasm and the optic tract. These studies could provide valuable insights into the physiological role of Wfs1 protein in astrocytes.

## Vision-related brain structures

***Superior colliculus.*** The superficial gray layer receives visual inputs directly from the retina and occipital cortex and contains cells that project extrinsically to dorsal thalamic nuclei (Edwards et al., 1986), whereas the intermediate gray layer receives indirect retinal inputs by way of the lateral division of the ventral lateral geniculate nucleus (Brauer and Schober, 1982). Wfs1-positive neurons in the intermediate gray layer as well as those in the superficial gray layer might be involved in visual functions. Neuropathological studies have demonstrated neuronal loss and gliosis in the SC of Wolfram syndrome patients (Genís et al., 1997; Shannon et al., 1999). These findings might be attributed to dysfunctional SC neurons in Wolfram syndrome patients due to loss-of-function mutations in the *WFS1* gene.

***Suprachiasmatic nucleus.*** The SCN is a circadian pacemaker. In the SCN, Wfs1-positive neurons were distributed in the dorsomedial region. This region does not receive direct retinal inputs, but does receive inputs from nonvisual sources. The region sends large numbers of axons to the hypothalamus and small numbers of axons to the thalamus, including the paraventricular thalamic nucleus (PVT). In the PVT, circadian timing information from the SCN is conveyed to multiple limbic structures including the amygdala and the limbic cortical areas (Watts and Swanson, 1987; Kawano et al., 2001; Leak and Moore, 2001). Thus, it is speculated that Wfs1-positive neurons in the dorsomedial part of the SCN provide circadian timing cues to the hypothalamus, the thalamus, and even to the multiple limbic structures without receiving direct retinal inputs.

***Visual cortex.*** The laminar distribution of Wfs1-positive neurons in layer II was present throughout the

mouse neocortex (Kawano et al., unpubl. obs.), as described in the rat (Takeda et al., 2001). Therefore, the distribution is not restricted to the visual cortex. Few thalamic afferents to the visual cortex terminate in layer II (afferents to V1 principally arise in the dorsal lateral geniculate nucleus; Peters and Feldman, 1976; afferents to V2 mainly arise in the lateral posterior nucleus; Olavarria, 1979), but associational afferents from other visual cortical areas terminate in layer II (Coogan and Burkhalter, 1990, 1993). Layer II neurons send associational fibers to the other visual cortical areas (Miller and Vogt, 1984a; Sanderson et al., 1991). Apart from the associational connections, the commissural neurons and terminals are concentrated in a narrow region (the border between V1 and V2L) where the vertical meridian is represented (Cipolloni and Peters, 1979; Cusick and Lund, 1981). In this region, layer II neurons send commissural fibers to and receive commissural fibers from the opposite cortex (Miller and Vogt, 1984b; Sefton et al., 1991). In addition, local circuit neurons are also located in layer II. These neurons make widespread connections within the same layer and project strongly to layer V (Burkhalter, 1989; Sefton and Dreher, 1995). Therefore, Wfs1-immunoreactive punctuations in layer V might be attributed to the strong projections from Wfs1-positive neurons in layer II to layer V. Further studies using tract-tracing methods are required to clarify the fiber connections of Wfs1-positive neurons in layer II. Neuroradiological and neuropathological studies have shown that there is mild cerebrocortical atrophy in Wolfram syndrome patients (Rando et al., 1992; Scolding et al., 1996; Shannon et al., 1999). The atrophy might be attributed to the dysfunctional cortical layer II neurons in Wolfram syndrome patients resulting from loss-of-function mutations in the *WFS1* gene.

## Optic atrophy

Optic atrophy is one of the minimal diagnostic criteria for Wolfram syndrome (Barrett et al., 1997). In this section we discuss the pathogenesis of optic atrophy in Wolfram syndrome based on the results obtained. Wfs1 was expressed in all neuron types (RGCs, amacrine cells, bipolar cells, horizontal cells, and photoreceptors) and Müller cells of the retina, in astrocytes of the optic nerve, and in neurons of the SC and the SCN. Out of these cells, candidates for causative cells for optic atrophy in Wolfram syndrome are not only RGCs but also amacrine cells, bipolar cells, SC neurons, SCN neurons, Müller cells, and astrocytes in the optic nerve, since it is speculated that candidate neurons express Wfs1 and are directly connected with RGCs and that cell bodies or axons of RGCs are surrounded by candidate glial cells.

First, we discuss whether RGCs are the principal candidates. In this case, autosomal dominant optic atrophy (ADOA) is useful for comparisons with Wolfram syndrome. ADOA is one of the primary inherited optic neuropathies, and has been attributed to mutations in the *OPA1* gene (Alexander et al., 2000; Delettre et al., 2000; Votruba et al., 2003). OPA1 protein expression is present in RGCs in the mouse, rat, and human (Aijaz et al., 2004; Pesch et al., 2004; Ju et al., 2005). The pattern electroretinogram (PERG) in ADOA patients shows an abnormal N95:P50 ratio, with a reduction in the amplitude of the N95 waveform (Berninger et al., 1991; Holder et al., 1998). Since the PERG N95 component is postulated to be specific for the retinal ganglion cell (Ryan and Arden, 1988), this finding supports a ganglion cell origin for ADOA (Votruba et al., 2003). By contrast, the ERG tests in Wolfram syndrome patients revealed normal or only slightly reduced responses, suggesting that the pathogenesis of the optic atrophy does not lie in the retina, but primarily affects the optic nerve (Niemeyer and Marquardt, 1972; Mtanda et al., 1986; Seynaeve et al., 1994; Barrett et al., 1997). In addition, Barrett et al. (1997) concluded that the reduced visual acuity not due to a refractive error and color vision defect suggested a site of pathology in the visual pathway proximal (posterior) to the eye. Thus, it is possible that the dysfunction of RGCs in Wolfram syndrome patients is mild and that the pathogenesis of optic atrophy is not attributable to the RGCs proper.

Previous clinical, pathological, and neurobiological studies weakly support the notion that amacrine cells, bipolar cells, SC neurons, SCN neurons, and Müller cells are the principal candidates. Although Wfs1 was expressed strongly in amacrine cells and weakly in bipolar cells, there have been few findings of functional abnormality in the INL of Wolfram syndrome patients by using ERGs (Niemeyer and Marquardt, 1972; Mtanda et al., 1986; Seynaeve et al., 1994; Barrett et al., 1997). In the mouse SC, Wfs1-positive cells were distributed in the superficial gray layer where retinal afferents terminate. In Wolfram syndrome patients, neuronal loss and gliosis are observed in the SC (Genís et al., 1997; Shannon et al., 1999). It is possible that optic atrophy is induced by retrograde degeneration of RGCs from the SC. In this case, the degenerated RGCs would be M-cells and K-cells (Y-cells and W-cells in the cat) not P-cells (X-cells in the cat; Garey, 1990; Goebel et al., 2004). By contrast, there is neuronal loss in the LGN mainly involving layers 3–6, which are P-cell relay layers (Garey, 1990; Genís et al., 1997; Goebel et al., 2004) or neuronal loss in all six layers of the LGN (Shannon et al., 1999). If SC neurons are the principal candidates, it is difficult to explain the loss of neurons in the LGN involving the P-cell relay layers. In the mouse SCN, Wfs1-positive neurons are distributed in the dorsomedial part where retinal afferents do not directly terminate. Since strong Wfs1 expression is present in Müller cells, and since RGCs are surrounded by Müller cells, there is a possibility that loss-of-function of Müller cells induces degeneration of RGCs in Wolfram syndrome patients. A neurobiological study using NSE-Hu-Bcl-2 transgenic mice demonstrated that early postnatal Müller cell death leads to retinal degeneration but not optic nerve degeneration (Dubois-Dauphin et al., 2000). It is improbable that Müller cells are the principal candidates. Thus, it is speculated that astrocytes in the optic nerve are the principal candidates for the causative cells for optic atrophy in Wolfram syndrome patients.

Since Wfs1 is expressed in many tissues, the reason why astrocytes in the optic nerve and not other cell types are principally affected by *WFS1* mutations which cause the optic atrophy in Wolfram syndrome is unknown. A biochemical study by using *Xenopus* oocytes suggested that WFS1 protein serves directly as a novel endoplasmic reticulum (ER) calcium channel or, alternatively, as a regulator of ER calcium channel activity. *WFS1* mutations associated with Wolfram syndrome reduce the susceptibility to cation block. It is possible that WFS1 protein-mediated regulation of intracellular calcium provides an important protective function in neurons and/or glial cells that are dependent on the ER for calcium signaling (Hay-

don, 2001; Osman et al., 2003). Recently, a functional study indicated that WFS1 protein expression increases in response to ER stress and that the protein plays a physiological role in protecting cells from ER stress-induced apoptosis (Ueda et al., 2005). Although the biochemical function of WFS1 in neurons and/or glial cells in the visual system remains to be investigated, it is possible that WFS1 mutations in the neurons and/or glial cells cause a disruption of the WFS1-mediated regulation of intracellular calcium levels and/or of the ER stress responses, and a consequent malfunction of electrophysiological activity in the neurons and/or glial cells (Haydon, 2001; Volterra and Meldolesi, 2005; Seifert et al., 2006). This loss-of-function may impair axons of RGCs leading to optic atrophy.

Wfs1 was localized to the afd part of the mouse optic nerve where GS immunoreactivity was almost negative (Figs. 6B, 8Q). This evidence suggests that a lack of GS in the afd part might augment the damage to the optic nerve caused by glutamate. Recently, vesicular glutamate release from axons was demonstrated not only in the corpus callosum but also in the optic nerve of rodents after the propagation of action potentials (Kukley et al., 2007; Ziskin et al., 2007). Thus, impaired glutamate clearance attributable to a lack of GS in the afd part may affect the viability of optic nerve axons in the mouse, including the *Wfs1* knockout mouse.

## CONCLUSION

In summary, Wfs1 was present not only in RGCs but also in photoreceptors, horizontal cells, bipolar cells, amacrine cells, and Müller cells of the retina, in astrocytes of the optic nerve, and in neurons of the SC, the SCN, and of the visual cortex. Interestingly, Wfs1 was localized to the afd part of the optic nerve where GS immunoreactivity was almost negative. These results suggest that mutant WFS1 may contribute to the dysfunction of WFS1-expressing neurons and/or glial cells, which may in turn lead to optic atrophy in Wolfram syndrome. They also suggest that the lack of GS in the afd part might augment the damage to the optic nerve caused by glutamate. Although these notions are difficult to test experimentally, the availability of the Wfs1 mouse model could offer opportunities for further investigation. These studies are required to determine the exact physiological role of Wfs1 protein in the biology of vision and to obtain more insights into its pathophysiological roles in optic atrophy in Wolfram syndrome.

## ACKNOWLEDGMENTS

The first and corresponding author, June Kawano, thanks Professor Shiro Nakagawa and Associate Professor Satoshi Kuchiiwa (Laboratory for Neuroanatomy, Department of Neurology, Kagoshima University Graduate School of Medical and Dental Sciences) for encouragement and for valuable discussions.

## LITERATURE CITED

Acar N, Gregoire S, Andre A, Juaneda P, Joffre C, Bron AM, Creuzot-Garcher CP, Bretillon L. 2007. Plasmalogens in the retina: in situ hybridization of dihydroxyacetone phosphate acyltransferase (DHAP-AT)—the first enzyme involved in their biosynthesis—and comparative study of retinal and retinal pigment epithelial lipid composition. Exp Eye Res 84:143–151.

Aijaz S, Erskine L, Jeffery G, Bhattacharya SS, Votruba M. 2004. Developmental expression profile of the optic atrophy gene product: OPA1 is not localized exclusively in the mammalian retinal ganglion cell layer. Invest Ophthalmol Vis Sci 45:1667–1673.

Alexander C, Votruba M, Pesch UE, Thiselton DL, Mayer S, Moore A, Rodriguez M, Kellner U, Leo-Kottler B, Auburger G, Bhattacharya SS, Wissinger B. 2000. *OPA1*, encoding a dynamin-related GTPase, is mutated in autosomal dominant optic atrophy linked to chromosome 3q28. Nat Genet 26:211–215.

Barrett TG, Bundey SE, Macleod AF. 1995. Neurodegeneration and diabetes: UK nationwide study of Wolfram (DIDMOAD) syndrome. Lancet 346:1458–1463.

Barrett TG, Bundey SE, Fielder AR, Good PA. 1997. Optic atrophy in Wolfram (DIDMOAD) syndrome. Eye 11:882–888.

Berninger TA, Jaeger W, Krastel H. 1991. Electrophysiology and colour perimetry in dominant infantile optic atrophy. Br J Ophthalmol 75:49–52.

Bitoun P. 1994. Wolfram syndrome. A report of four cases and review of the literature. Ophthalmic Genet 15:77–85.

Brandstätter JH, Greferath U, Euler T, Wässle H. 1995. Co-stratification of $GABA_A$ receptors with the directionally selective circuitry of the rat retina. Vis Neurosci 12:345–358.

Brauer K, Schober W. 1982. Identification of geniculo-tectal relay neurons in the rat's ventral lateral geniculate nucleus. Exp Brain Res 45:84–88.

Brecha N, Johnson D, Peichl L, Wässle H. 1988. Cholinergic amacrine cells of the rabbit retina contain glutamate decarboxylase and g-aminobutyrate immunoreactivity. Proc Natl Acad Sci U S A 85:6187–6191.

Bringmann A, Reichenbach A. 2001. Role of Müller cells in retinal degenerations. Front Biosci 6:E72–92.

Brown SP, Masland RH. 1999. Costratification of a population of bipolar cells with the direction-selective circuitry of the rabbit retina. J Comp Neurol 408:97–106.

Bumsted K, Jasoni C, Szél A, Hendrickson A. 1997. Spatial and temporal expression of cone opsins during monkey retinal development. J Comp Neurol 378:117–134.

Burkhalter A. 1989. Intrinsic connections of rat primary visual cortex: laminar organization of axonal projections. J Comp Neurol 279:171–186.

Cipolloni PB, Peters A. 1979. The bilaminar and banded distribution of the callosal terminals in the posterior neocortex of the rat. Brain Res 176:33–47.

Collier DA, Barrett TG, Curtis D, Macleod A, Arranz MJ, Maassen JA, Bundey S. 1996. Linkage of Wolfram syndrome to chromosome 4p16.1 and evidence for heterogeneity. Am J Hum Genet 59:855–863.

Coogan TA, Burkhalter A. 1990. Conserved patterns of cortico-cortical connections define areal hierarchy in rat visual cortex. Exp Brain Res 80:49–53.

Coogan TA, Burkhalter A. 1993. Hierarchical organization of areas in rat visual cortex. J Neurosci 13:3749–3772.

Cowlen MS, Zhang VZ, Warnock L, Moyer CF, Peterson WM, Yerxa BR. 2003. Localization of ocular $P2Y_2$ receptor gene expression by in situ hybridization. Exp Eye Res 77:77–84.

Cryns K, Thys S, Van Laer L, Oka Y, Pfister M, Van Nassauw L, Smith RJ, Timmermans JP, Van Camp G. 2003. The *WFS1* gene, responsible for low frequency sensorineural hearing loss and Wolfram syndrome, is expressed in a variety of inner ear cells. Histochem Cell Biol 119:247–256.

Cusick CG, Lund RD. 1981. The distribution of the callosal projection to the occipital visual cortex in rats and mice. Brain Res 214:239–259.

Dacey DM, Lee BB, Stafford DK, Pokorny J, Smith VC. 1996. Horizontal cells of the primate retina: cone specificity without spectral opponency. Science 271:656–659.

Debus E, Weber K, Osborn M. 1983. Monoclonal antibodies specific for glial fibrillary acidic (GFA) protein and for each of the neurofilament triplet polypeptides. Differentiation 25:193–203.

Delettre C, Lenaers G, Griffoin JM, Gigarel N, Lorenzo C, Belenguer P, Pelloquin L, Grosgeorge J, Turc-Carel C, Perret E, Astarie-Dequeker C, Lasquellec L, Arnaud B, Ducommun B, Kaplan J, Hamel CP. 2000. Nuclear gene *OPA1*, encoding a mitochondrial dynamin-related protein, is mutated in dominant optic atrophy. Nat Genet 26:207–210.

Dráberová E, Lukás Z, Ivanyi D, Viklicky V, Dráber P. 1998. Expression of

class III β-tubulin in normal and neoplastic human tissues. Histochem Cell Biol 109:231–239.

Dräger UC. 1983. Coexistence of neurofilaments and vimentin in a neurone of adult mouse retina. Nature 303:169–172.

Dubois-Dauphin M, Poitry-Yamate C, de Bilbao F, Julliard AK, Jourdan F, Donati G. 2000. Early postnatal Müller cell death leads to retinal but not optic nerve degeneration in NSE-Hu-Bcl-2 transgenic mice. Neuroscience 95:9–21.

Edwards MA, Caviness VS Jr, Schneider GE. 1986. Development of cell and fiber lamination in the mouse superior colliculus. J Comp Neurol 248:395–409.

Euler T, Detwiler PB, Denk W. 2002. Directionally selective calcium signals in dendrites of starburst amacrine cells. Nature 418:845–852.

Fried SI, Munch TA, Werblin FS. 2002. Mechanisms and circuitry underlying directional selectivity in the retina. Nature 420:411–414.

Friedman B, Hockfield S, Black JA, Woodruff KA, Waxman SG. 1989. In situ demonstration of mature oligodendrocytes and their processes: an immunocytochemical study with a new monoclonal antibody, rip. Glia 2:380–390.

Fujinaga R, Kawano J, Matsuzaki Y, Kamei K, Yanai A, Sheng Z, Tanaka M, Nakahama K, Nagano M, Shinoda K. 2004. Neuroanatomical distribution of Huntingtin-associated protein 1-mRNA in the male mouse brain. J Comp Neurol 478:88–109.

Garey LJ. 1990. Visual system. In: Paxinos G, editor. The human nervous system. San Diego: Academic Press. p 945–977.

Gargini C, Terzibasi E, Mazzoni F, Strettoi E. 2007. Retinal organization in the retinal degeneration 10 (rd10) mutant mouse: a morphological and ERG study. J Comp Neurol 500:222–238.

Genís D, Dávalos A, Molins A, Ferrer I. 1997. Wolfram syndrome: a neuropathological study. Acta Neuropathol (Berl) 93:426–429.

Goebel R, Muckli L, Kim DS. 2004. Visual system. In: Paxinos G, Mai JK, editors. The human nervous system. San Diego: Elsevier Academic Press. p 1280–1305.

Gómez-Zaera M, Strom TM, Rodríguez B, Estivill X, Meitinger T, Nunes V. 2001. Presence of a major WFS1 mutation in Spanish Wolfram syndrome pedigrees. Mol Genet Metab 72:72–81.

Hardy C, Khanim F, Torres R, Scott-Brown M, Seller A, Poulton J, Collier D, Kirk J, Polymeropoulos M, Latif F, Barrett T. 1999. Clinical and molecular genetic analysis of 19 Wolfram syndrome kindreds demonstrating a wide spectrum of mutations in WFS1. Am J Hum Genet 65:1279–1290.

Haverkamp S, Wässle H. 2000. Immunocytochemical analysis of the mouse retina. J Comp Neurol 424:1–23.

Haydon PG. 2001. GLIA: listening and talking to the synapse. Nat Rev Neurosci 2:185–193.

Hofmann S, Philbrook C, Gerbitz KD, Bauer MF. 2003. Wolfram syndrome: structural and functional analyses of mutant and wild-type wolframin, the WFS1 gene product. Hum Mol Genet 12:2003–2012.

Holder GE, Votruba M, Carter AC, Bhattacharya SS, Fitzke FW, Moore AT. 1998. Electrophysiological findings in dominant optic atrophy (DOA) linking to the OPA1 locus on chromosome 3q 28-qter. Doc Ophthalmol 95:217–228.

Inoue H, Tanizawa Y, Wasson J, Behn P, Kalidas K, Bernal-Mizrachi E, Mueckler M, Marshall H, Donis-Keller H, Crock P, Rogers D, Mikuni M, Kumashiro H, Higashi K, Sobue G, Oka Y, Permutt MA. 1998. A gene encoding a transmembrane protein is mutated in patients with diabetes mellitus and optic atrophy (Wolfram syndrome). Nat Genet 20:143–148.

Ishihara H, Takeda S, Tamura A, Takahashi R, Yamaguchi S, Takei D, Yamada T, Inoue H, Soga H, Katagiri H, Tanizawa Y, Oka Y. 2004. Disruption of the *WFS1* gene in mice causes progressive β-cell loss and impaired stimulus-secretion coupling in insulin secretion. Hum Mol Genet 13:1159–1170.

Jalil MA, Begum L, Contreras L, Pardo B, Iijima M, Li MX, Ramos M, Marmol P, Horiuchi M, Shimotsu K, Nakagawa S, Okubo A, Sameshima M, Isashiki Y, Del Arco A, Kobayashi K, Satrústegui J, Saheki T. 2005. Reduced *N*-acetylaspartate levels in mice lacking aralar, a brain- and muscle-type mitochondrial aspartate-glutamate carrier. J Biol Chem 280:31333–31339.

Jeon CJ, Strettoi E, Masland RH. 1998. The major cell populations of the mouse retina. J Neurosci 18:8936–8946.

Ju WK, Misaka T, Kushnareva Y, Nakagomi S, Agarwal N, Kubo Y, Lipton SA, Bossy-Wetzel E. 2005. OPA1 expression in the normal rat retina and optic nerve. J Comp Neurol 488:1–10.

Kang TH, Ryu YH, Kim IB, Oh GT, Chun MH. 2004. Comparative study of cholinergic cells in retinas of various mouse strains. Cell Tissue Res 317:109–115.

Kawano J, Krout KE, Loewy AD. 2001. Suprachiasmatic nucleus projections to the paraventricular thalamic nucleus of the rat. Thalamus Relat Syst 1:197–202.

Khanim F, Kirk J, Latif F, Barrett TG. 2001. WFS1/wolframin mutations, Wolfram syndrome, and associated diseases. Hum Mutat 17:357–367.

Kukley M, Capetillo-Zarate E, Dietrich D. 2007. Vesicular glutamate release from axons in white matter. Nat Neurosci 10:311–320.

Leak RK, Moore RY. 2001. Topographic organization of suprachiasmatic nucleus projection neurons. J Comp Neurol 433:312–334.

Miller MW, Vogt BA. 1984a. Direct connections of rat visual cortex with sensory, motor, and association cortices. J Comp Neurol 226:184–202.

Miller MW, Vogt BA. 1984b. Heterotopic and homotopic callosal connections in rat visual cortex. Brain Res 297:75–89.

Minton JA, Rainbow LA, Ricketts C, Barrett TG. 2003. Wolfram syndrome. Rev Endocr Metab Disord 4:53–59.

Morcos Y, Chan-Ling T. 2000. Concentration of astrocytic filaments at the retinal optic nerve junction is coincident with the absence of intraretinal myelination: comparative and developmental evidence. J Neurocytol 29:665–678.

Mtanda AT, Cruysberg JR, Pinckers AJ. 1986. Optic atrophy in Wolfram syndrome. Ophthalmic Paediatr Genet 7:159–165.

Neufeld AH. 1999. Microglia in the optic nerve head and the region of parapapillary chorioretinal atrophy in glaucoma. Arch Ophthalmol 117:1050–1056.

Niemeyer G, Marquardt JL. 1972. Retinal function in an unique syndrome of optic atrophy, juvenile diabetes mellitus, diabetes insipidus, neurosensory hearing loss, autonomic dysfunction, and hyperalanineuria. Invest Ophthalmol 11:617–624.

Nogami H, Ogasawara K, Mimura Y, Mogi K, Shutoh F, Hisano S. 2006. Developmentally-regulated expression of tissue-specific splice variant of rat vesicular glutamate transporter 1 in retina and pineal gland. J Neurochem 99:142–153.

Olavarria J. 1979. A horseradish peroxidase study of the projections from the latero-posterior nucleus to three lateral peristriate areas in the rat. Brain Res 173:137–141.

Ölveczky BP, Baccus SA, Meister M. 2003. Segregation of object and background motion in the retina. Nature 423:401–408.

Osman AA, Saito M, Makepeace C, Permutt MA, Schlesinger P, Mueckler M. 2003. Wolframin expression induces novel ion channel activity in endoplasmic reticulum membranes and increases intracellular calcium. J Biol Chem 278:52755–52762.

Paxinos G, Franklin KBJ. 2001. The mouse brain in stereotaxic coordinates. San Diego: Academic Press.

Pesch UE, Fries JE, Bette S, Kalbacher H, Wissinger B, Alexander C, Kohler K. 2004. *OPA1*, the disease gene for autosomal dominant optic atrophy, is specifically expressed in ganglion cells and intrinsic neurons of the retina. Invest Ophthalmol Vis Sci 45:4217–4225.

Peters A, Feldman ML. 1976. The projection of the lateral geniculate nucleus to area 17 of the rat cerebral cortex. I. General description. J Neurocytol 5:63–84.

Polymeropoulos MH, Swift RG, Swift M. 1994. Linkage of the gene for Wolfram syndrome to markers on the short arm of chromosome 4. Nat Genet 8:95–97.

Rando TA, Horton JC, Layzer RB. 1992. Wolfram syndrome: evidence of a diffuse neurodegenerative disease by magnetic resonance imaging. Neurology 42:1220–1224.

Reichert F, Rotshenker S. 1996. Deficient activation of microglia during optic nerve degeneration. J Neuroimmunol 70:153–161.

Roska B, Werblin F. 2001. Vertical interactions across ten parallel, stacked representations in the mammalian retina. Nature 410:583–587.

Ryan S, Arden GB. 1988. Electrophysiological discrimination between retinal and optic nerve disorders. Doc Ophthalmol 68:247–255.

Saari JC, Huang J, Possin DE, Fariss RN, Leonard J, Garwin GG, Crabb JW, Milam AH. 1997. Cellular retinaldehyde-binding protein is expressed by oligodendrocytes in optic nerve and brain. Glia 21:259–268.

Sanderson KJ, Dreher B, Gayer N. 1991. Prosencephalic connections of striate and extrastriate areas of rat visual cortex. Exp Brain Res 85:324–334.

Scolding NJ, Kellar-Wood HF, Shaw C, Shneerson JM, Antoun N. 1996. Wolfram syndrome: hereditary diabetes mellitus with brainstem and optic atrophy. Ann Neurol 39:352–360.

Sefton AJ, Dreher B. 1995. Visual system. In: Paxinos G, editor. The rat nervous system. San Diego: Academic Press. p 833–898.

Sefton AJ, Dreher B, Lim WL. 1991. Interactions between callosal, thalamic and associational projections to the visual cortex of the developing rat. Exp Brain Res 84:142–158.

Seifert G, Schilling K, Steinhäuser C. 2006. Astrocyte dysfunction in neurological disorders: a molecular perspective. Nat Rev Neurosci 7:194–206.

Seynaeve H, Vermeiren A, Leys A, Dralands L. 1994. Four cases of Wolfram syndrome: ophthalmologic findings and complications. Bull Soc Belge Ophtalmol 252:75–80.

Shannon P, Becker L, Deck J. 1999. Evidence of widespread axonal pathology in Wolfram syndrome. Acta Neuropathol (Berl) 98:304–308.

Sharma RK, Netland PA. 2007. Early born lineage of retinal neurons express class III β-tubulin isotype. Brain Res 1176:11–17.

Sheng Z, Kawano J, Yanai A, Fujinaga R, Tanaka M, Watanabe Y, Shinoda K. 2004. Expression of estrogen receptors (α, β) and androgen receptor in serotonin neurons of the rat and mouse dorsal raphe nuclei; sex and species differences. Neurosci Res 49:185–196.

Strom TM, Hörtnagel K, Hofmann S, Gekeler F, Scharfe C, Rabl W, Gerbitz KD, Meitinger T. 1998. Diabetes insipidus, diabetes mellitus, optic atrophy and deafness (DIDMOAD) caused by mutations in a novel gene (*wolframin*) coding for a predicted transmembrane protein. Hum Mol Genet 7:2021–2028.

Takeda K, Inoue H, Tanizawa Y, Matsuzaki Y, Oba J, Watanabe Y, Shinoda K, Oka Y. 2001. WFS1 (Wolfram syndrome 1) gene product: predominant subcellular localization to endoplasmic reticulum in cultured cells and neuronal expression in rat brain. Hum Mol Genet 10:477–484.

Takei D, Ishihara H, Yamaguchi S, Yamada T, Tamura A, Katagiri H, Maruyama Y, Oka Y. 2006. WFS1 protein modulates the free $Ca^{2+}$ concentration in the endoplasmic reticulum. FEBS Lett 580:5635–5640.

Taylor WR, Vaney DI. 2002. Diverse synaptic mechanisms generate direction selectivity in the rabbit retina. J Neurosci 22:7712–7720.

Taylor WR, Vaney DI. 2003. New directions in retinal research. Trends Neurosci 26:379–385.

Tessa A, Carbone I, Matteoli MC, Bruno C, Patrono C, Patera IP, De Luca F, Lorini R, Santorelli FM. 2001. Identification of novel WFS1 mutations in Italian children with Wolfram syndrome. Hum Mutat 17:348–349.

Ueda K, Kawano J, Takeda K, Yujiri T, Tanabe K, Anno T, Akiyama M, Nozaki J, Yoshinaga T, Koizumi A, Shinoda K, Oka Y, Tanizawa Y. 2005. Endoplasmic reticulum stress induces Wfs1 gene expression in pancreatic β-cells via transcriptional activation. Eur J Endocrinol 153: 167–176.

Voigt T. 1986. Cholinergic amacrine cells in the rat retina. J Comp Neurol 248:19–35.

Volterra A, Meldolesi J. 2005. Astrocytes, from brain glue to communication elements: the revolution continues. Nat Rev Neurosci 6:626–640.

von Gräfe A. 1858. Über die mit Diabetes vorkommenden Sehstörungen. Arch Ophthal 4:230–234.

Votruba M, Aijaz S, Moore AT. 2003. A review of primary hereditary optic neuropathies. J Inherit Metab Dis 26:209–227.

Warr WB, de Olmos JS, Heimer L. 1981. Horseradish peroxidase: the basic procedure. In: Heimer L, Robards MJ, editors. Neuroanatomical tract-tracing methods. New York: Plenum Press. p 207–262.

Wässle H. 2004. Parallel processing in the mammalian retina. Nat Rev Neurosci 5:747–757.

Watts AG, Swanson LW. 1987. Efferent projections of the suprachiasmatic nucleus: II. Studies using retrograde transport of fluorescent dyes and simultaneous peptide immunohistochemistry in the rat. J Comp Neurol 258:230–252.

Wolfram DJ, Wagener HP. 1938. Diabetes mellitus and simple optic atrophy among siblings: report of four cases. Mayo Clin Proc 13:715–718.

Xiang M, Zhou L, Macke JP, Yoshioka T, Hendry SH, Eddy RL, Shows TB, Nathans J. 1995. The Brn-3 family of POU-domain factors: primary structure, binding specificity, and expression in subsets of retinal ganglion cells and somatosensory neurons. J Neurosci 15:4762–4785.

Yamaguchi S, Ishihara H, Tamura A, Yamada T, Takahashi R, Takei D, Katagiri H, Oka Y. 2004. Endoplasmic reticulum stress and N-glycosylation modulate expression of WFS1 protein. Biochem Biophys Res Commun 325:250–256.

Yamamoto H, Hofmann S, Hamasaki DI, Kreczmanski P, Schmitz C, Parel JM, Schmidt-Kastner R. 2006. Wolfram syndrome 1 (WFS1) protein expression in retinal ganglion cells and optic nerve glia of the cynomolgus monkey. Exp Eye Res 83:1303–1306.

Yoshida K, Watanabe D, Ishikane H, Tachibana M, Pastan I, Nakanishi S. 2001. A key role of starburst amacrine cells in originating retinal directional selectivity and optokinetic eye movement. Neuron 30:771–780.

Ziskin JL, Nishiyama A, Rubio M, Fukaya M, Bergles DE. 2007. Vesicular release of glutamate from unmyelinated axons in white matter. Nat Neurosci 10:321–330.

Biochemical and Biophysical Research Communications 369 (2008) 1204–1208

Contents lists available at ScienceDirect

Biochemical and Biophysical Research Communications

journal homepage: www.elsevier.com/locate/ybbrc

# Identification of Glypican3 as a novel GLUT4-binding protein

Akihiko Taguchi [a], Masahiro Emoto [a], Shigeru Okuya [a,*], Naofumi Fukuda [a], Yoshitaka Nakamori [a], Mutsuko Miyazaki [a], Sachiko Miyamoto [a], Katsuya Tanabe [a], Hiroyuki Aburatani [b], Yoshitomo Oka [c], Yukio Tanizawa [a]

[a] Division of Endocrinology, Metabolism, Hematological Sciences and Therapeutics, Department of Bio-Signal Analysis, Yamaguchi University Graduate School of Medicine, 1-1-1 Minami-Kogushi, Ube, Yamaguchi, Japan
[b] Genome Science Division, Research Center for Advanced Science and Technology, University of Tokyo, Tokyo, Japan
[c] Division of Molecular Metabolism and Diabetes, Tohoku University Graduate School of Medicine, Sendai 980-8575, Japan

ARTICLE INFO

*Article history:*
Received 5 March 2008
Available online 14 March 2008

*Keywords:*
GLUT4
3T3-L1 Adipocytes
GPC3

ABSTRACT

Insulin stimulates glucose uptake in fat and muscle primarily by stimulating the translocation of vesicles containing facilitative glucose transporters, GLUT4, from intracellular compartments to the plasma membrane. Although cell surface externalization of GLUT4 is critical for glucose transport, the mechanism regulating cell surface GLUT4 remains unknown. Using a yeast two-hybrid screening system, we have screened GLUT4-binding proteins, and identified a novel glycosyl phosphatidyl inositol (GPI)-linked proteoglycan, Glypican3 (GPC3). We confirmed their interaction using immunoprecipitation and a GST pull-down assay. We also revealed that GPC3 and GLUT4 to co-localized at the plasma membrane, using immunofluorescent microscopy. Furthermore, we observed that glucose uptake in GPC3-overexpressing adipocytes was increased by 30% as compared to control cells. These findings suggest that GPC3 may play roles in glucose transport through GLUT4.



Insulin stimulation of glucose uptake into skeletal muscle and adipose tissue is achieved via the translocation of intracellular-sequestered GLUT4 protein to the cell surface membrane [1,2]. On the plasma membrane, GLUT4 proteins, responding to insulin stimulation, remain externalized for a certain period of time and facilitate glucose transport. Although cell surface externalization of GLUT4 is critical for glucose transport, the mechanism regulating cell surface GLUT4 remains largely unknown. We speculated that it would require a protein capable of interacting with the glucose transporter.

Over the past decade, several GLUT4-binding proteins, such as mUbc9 [3], TUG [4], DAXX [5], L-3-hydroxyacyl-CoA dehydrogenase [6], and carboxyl esterase [7], have been identified using the C-terminus region of GLUT4 as bait in either a two-hybrid system or an immobilized GST fusion protein pull-down experiment. For example, mUbc9 was demonstrated to regulate transporter degradation [3], whereas TUG was shown to modulate GLUT4 distribution [4]. However, the functions of other GLUT4-binding proteins are not fully understood. We speculated that a change in the three-dimensional structure of the GLUT4 partial sequence has made it difficult to identify and analyze functional GLUT4 binding proteins. Thus, we used full-length GLUT4 for screening, and thereby identified GPC3 as a GLUT4-binding protein.

GPC3 is one of the heparan sulfate proteoglycans that are anchored to the cell membrane by a glycosyl-phosphatidylinositol protein [8]. This family of proteins was shown to be related to morphogenesis and GPC3 was originally reported to be a negative regulator of cell proliferation as well as the progression of malignant tumors [9–13]. Herein, we report GPC3 as a newly identified GLUT4-binding protein. This is the first report describing a protein that acts directly on GLUT4 molecules at the plasma membrane.

## Materials and methods

*Antibodies.* Mouse monoclonal GPC3 antibody was provided by Dr. Hiroyuki Aburatani (University of Tokyo, Japan). The following antibodies were used: anti-GLUT4 rabbit and goat, anti-GST (Santa Cruz Biotechnology, CA); anti-FLAG (M2) (Sigma); anti-Myc (9E10) (Convance, CA) and fluorescent-conjugated and horseradish peroxidase-conjugated secondary antibodies (Jackson Immuno-Research Laboratories).

*Constructs.* Mouse GPC3 cDNA was purchased from Open Biosystems (Huntsville, AL). Wild-type GPC3 was subcloned into a pGEX-6P1 (GE Healthcare Biosciences) vector. FLAG-tagged GPC3 and 4×Myc-tagged GLUT4-eGFP was subcloned into a pcDNA3 (Invitrogen) vector. All chemically synthesized and PCR-derived DNA sequences were verified by DNA sequencing.

*Preparation of recombinant adenovirus vectors.* Recombinant adenovirus encoding eGFP or FLAG-tagged GPC3 was constructed using the AdEasy adenovirus vector system according to the manufacturer's instructions (Startagene). All amplified viruses were stored at −80 °C. 3T3-L1 adipocytes were infected with recombinant adenovirus vectors encoding eGFP and FLAG-tagged GPC3 at a multiplicity of infection (m.o.i.) of 50.

* Corresponding author. Fax: +81 836 22 2342.
*E-mail address:* okuya@yamaguchi-u.ac.jp (S. Okuya).

0006-291X/$ - see front matter © 2008 Elsevier Inc. All rights reserved.
doi:10.1016/j.bbrc.2008.03.027

*Cell culture.* 3T3-L1 fibroblasts were grown in DMEM with 10% fetal bovine serum (FBS) at 37 °C. The cells (3–5 days post-confluent) were differentiated into adipocytes by incubation in the same DMEM containing 0.5 mM isobutylmethylxanthine, 0.25 μM dexamethasone, and 4 μg/ml insulin for 3 days, and then grown in DMEM with 10% FBS for an additional 3–6 days. Human hepatocellular carcinoma cell line HepG2 cells were cultured in Eagle's minimum essential medium (EMEM) with 10% FBS in at 37 °C.

*Primary culture of mouse hepatocytes.* Mouse hepatocytes were prepared from 5-month male C57BL/6J mice as described previously [14]. Isolated cells were seeded onto coverslips and allowed to recover for 24 h.

*Yeast two-hybrid screening.* The MATCHMAKER LexA Two-hybrid System (Clontech) was used for identification of GLUT4-binding proteins. As bait for screening, the vector pLexA-GLUT4 expressing a fusion protein composed of full-length rat GLUT4 linked to the DNA-binding domain was constructed. A rat adipocyte cDNA library already cloned into the pB42AD vector was obtained from Origene Technologies (Rockville, MD). Approximately 300 colonies showed activation of the yeast reporter gene, and 15 colonies showing dependence on the LexA-GLUT4 fusion protein for activation of the reporter gene were selected. Plasmids from positive clones were subsequently isolated from the yeast, transferred to E. coli, and sequenced. Full-length cDNA was obtained by 5′RACE (Rapid Amplification of cDNA End) using a kit (Clontech) and the GenBank/NCBI databases were screened for similar sequences using BLAST Search.

*In vitro GST pull-down assay.* GST fusion proteins of full-length GPC3 and GST alone were purified according to the manufacturer's instructions. GLUT4 protein was generated from Myc-tagged GLUT4-eGFP (four-Myc epitope-tags in the first exofacial loop and eGFP in the C-terminus) transfected 293 cells and further purified using anti-Myc antibody. These GST fusion proteins and purified 4×Myc-tagged GLUT4-eGFP were mixed in PBS and incubated at 4 °C for 4 h. The proteins were then pulled down with glutathione–sepharose beads (GE Healthcare Biosciences).

*Immunoprecipitation and immunoblotting.* Cells were lysed in lysis buffer [20 mM Hepes (pH 7.2), 100 mM NaCl, 1 mM EDTA, 25 mM NaF, 1 mM sodium vanadate, 1 mM benzamidine, 5 μg/ml leupeptin, 5 μg/ml aprotinin, 1 mM PMSF, and 1 mM DTT] and the protein concentration was measured with BCA protein assay reagent (Pierce, Rockford, IL). For immunoprecipitation, the cell lysate was pre-incubated with protein-G Sepharose at 4 °C for 30 min to remove non-specific bound proteins. Then, samples were incubated with primary antibody at 4 °C for 8–12 h followed by incubation with protein-G Sepharose. Lysates and immunoprecipitates were resolved by SDS–PAGE and transferred to a polyvinylidene difluoride (PVDF) membrane (GE Healthcare Biosciences). The membranes were incubated with appropriate antibodies.

*Immunofluorescence microscopy.* 3T3-L1 adipocytes, HepG2 cells, and primary hepatocytes were seeded onto coverslips and allowed to recover for 24–48 h. 3T3-L1 adipocytes were serum-starved for 4 h in DMEM, followed by incubation with or without 100 nM of insulin for 15 min at 37 °C. Then, all of the cells were fixed with 3.7% formaldehyde in PBS and permeabilized with buffer A (0.5% Triton X-100 and 1% FBS in PBS) for 15 min, and finally incubated for 2 h with primary antibodies at room temperature. The cells were washed and incubated with an appropriate secondary antibody, or rhodamine-conjugated wheat germ agglutinin (Molecular Probes, Inc.) as a counter staining of cell membrane and Golgi system. The coverslips were washed thoroughly and mounted on glass slides. Immunostained cells were observed at room temperature with a laser-scanning confocal microscope (LSM5 PASCAL; Carl Zeiss Inc.).

*Plasma membrane sheet assay.* Cell surface protein was assayed using plasma membrane lawns as described previously [15]. The cells were subsequently swollen using hypotonic buffer and sonicated to generate a lawn of plasma membrane fragments. The membranes were immunostained with anti-GPC3 and anti-GLUT4 antibody. These cells were observed by laser confocal microscopy.

*2-Deoxy-glucose uptake.* Differentiated adipocytes were prepared in 24-well plates. Cells were infected with the recombinant adenoviruses. Two days thereafter, the cells were serum-starved for 2 h at 37 °C in Krebs–Ringer phosphate buffer (130 mM NaCl, 5 mM KCl, 1.3 mM $CaCl_2$, 1.3 mM $MgSO_4$, and 10 mM $Na_2HPO_4$, pH 7.4). The cells were then stimulated with or without 100 nM of insulin for 15 min, and deoxy-glucose uptake was determined by 2-deoxy-D-[2,6$^3$H] glucose incorporation.

## Results and discussion

### *Identification of GLUT4-binding proteins*

Regulation of glucose uptake in muscle and adipose tissues by insulin is important for proper maintenance of blood glucose. This hormone stimulates translocation of the GLUT4 glucose transporter from the intracellular membrane to the cell surface. After translocation to the plasma membrane, GLUT4 remains on the cell surface temporarily and facilitates glucose transport. However, the mechanism regulating cell surface GLUT4 is still largely unknown. We hypothesized that it requires protein–protein interactions at the plasma membrane. We used the yeast two-hybrid screening system to identify proteins that interact physically with full-length GLUT4. As bait, we used full-length rat GLUT4 cDNA and, as prey, a rat adipose tissue cDNA library. After the first screening, we obtained more than 300 colonies. After a second screening, 15 colonies remained positive. Ultimately, nine colonies were left. Full-length cDNAs were obtained by 5′RACE. One of them was 100% identical to GPC3 [16], which was originally cloned as OCI-5, a GPI anchored membrane protein [17]. Since we also obtained mUbc9 [3], which was previously identified using the same method, our experimental procedure was thought to have worked correctly. The GPC3 sequence obtained with the yeast two-hybrid system was comprised of the residues from 521 to 597. In order to confirm the interaction between GLUT4 and GPC3, we employed the yeast two-hybrid system again; using full-length GLUT4 cDNA and full-length GPC3 cDNA as the bait and prey, respectively. We confirmed the LacZ signal indicating a direct interaction between GPC3 and GLUT4 (Fig. 1A). Next, we determined GPC3 protein expression using Western blot analysis. As shown in Fig. 1B, we detected high molecular weight form corresponding to the glycosylated GPC3 and bands corresponding to the non-glycosylated GPC3 core protein and its cleavage product of in 3T3-L1 adipocytes as in HepG2 cells. These data were consistent with the previous reports [11,13].

### *Intracellular localization of GPC3*

The intracellular localization of GPC3 was observed in adipocytes by laser confocal microscopy. First, we determined GPC3 protein by immunofluorescent microscopy using our specific antibody against GPC3 in HepG2 cells and primary hepatocytes as a positive or negative control, respectively (Fig. 2A). As shown in Fig. 2B, most of the GPC3 was at the plasma membrane, as reported for other cell lines [17]. As expected, we observed co-localization of GLUT4 and GPC3 after insulin stimulation (Fig. 2B). Next, in order to confirm plasma membrane integrity, we prepared plasma membrane sheets from 3T3-L1 adipocytes, stained with anti-GPC3 and anti-GLUT4 antibodies, and then observed GPC3 expression by confocal microscopy (Fig. 2C). We observed that GLUT4 translocated to the plasma membrane in response to insulin stimulation. GPC3 localized at the plasma membrane on under both conditions, and merged more clearly with GLUT4 after insulin stimulation.

The results shown in Fig. 1A and Fig. 2 suggest that GPC3 interacted with GLUT4 at the plasma membrane.

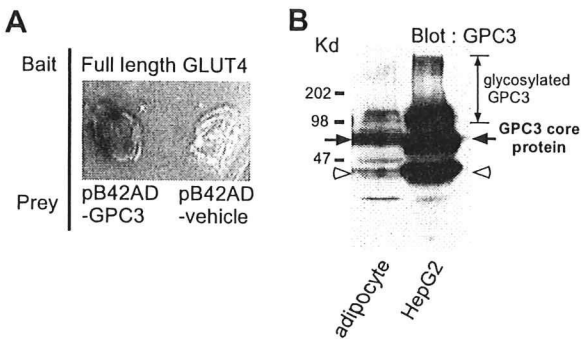


**Fig. 1.** Identification and expression profile of GPC3. (A) Interaction between GLUT4 and GPC3 was confirmed by the yeast two-hybrid system. Full-length cDNAs of GLUT4 and GPC3 were used as bait and prey, respectively. (B) Lysates of 3T3-L1 adipocytes and HepG2 cells were prepared, and separated by SDS-PAGE. The membrane was then blotted with anti-GPC3 antibody. HepG2 lysate was used as positive control. Arrow indicates the non-glycosylated full-length GPC3 core protein. Open arrowhead indicates a cleavage product containing the N-terminus of GPC3.

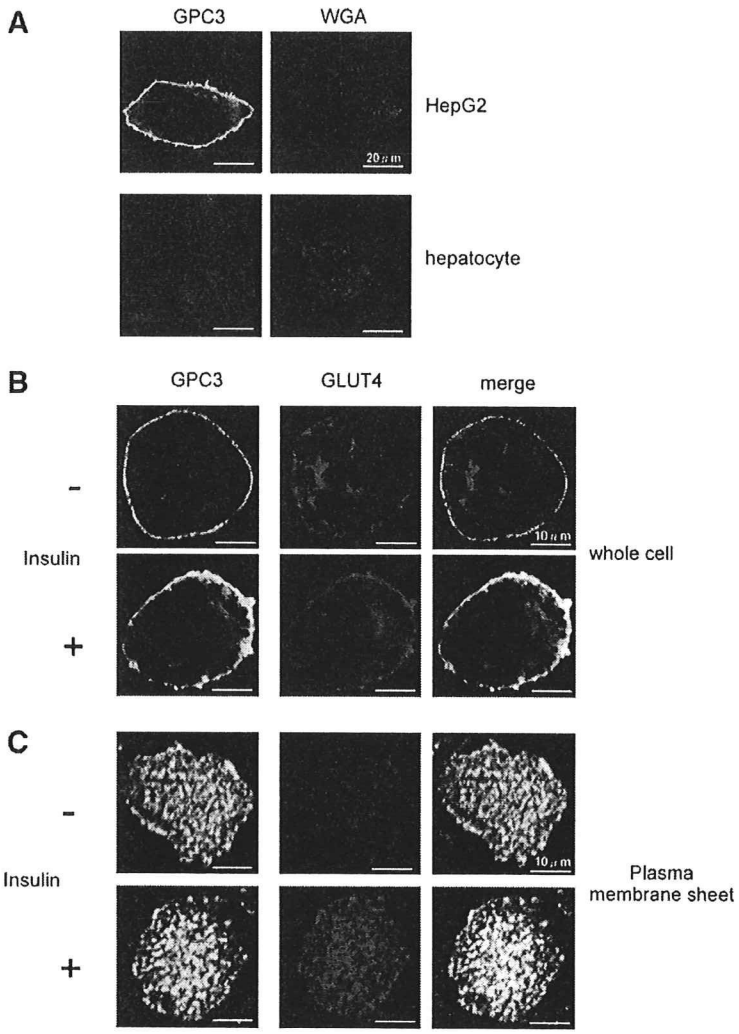


**Fig. 2.** Intracellular localization of GPC3. (A) Primary hepatocytes and HepG2 cells were plated on cover slips. These cells were fixed with formaldehyde and then stained using anti-GPC3 antibody followed by FITC-labeled secondary antibody. Rhodamine-conjugated wheat germ agglutinin (WGA) was used as counter staining of cell membrane and Golgi system. (B) 3T3-L1 adipocytes were serum-starved for 3-4 h and treated with or without 100 nM of insulin for 20 min. The cells were fixed with formaldehyde and stained using anti-GPC3 and anti-GLUT4 antibodies followed by appropriate FITC or Cy3 labeled secondary antibodies. These cells were observed by laser confocal microscopy. (C) 3T3-L1 adipocytes cultured on glass coverslips were treated with or without 100 nM of insulin for 15 min. At the end of each experiment, cells were rapidly washed in PBS followed by a 40 s treatment in PBS containing 0.5 mg/ml poly-L-lysine (Sigma). The cells were subsequently swollen using hypotonic buffer and sonicated to generate a lawn of plasma membrane fragments. The membranes were immunostained with anti-GPC3 and anti-GLUT4 antibody. Stained cells were observed using the confocal microscopy system as described above.

*Interaction between GLUT4 and GPC3*

In order to reconfirm the interaction between GPC3 and GLUT4, we conducted two other experiments; immunoprecipitation and a GST pull-down assay. First, we examined endogenous protein–protein interactions employing immunoprecipitation experiments. We prepared the total lysates of insulin-treated 3T3-L1 adipocytes. These lysates were immunoprecipitated with anti-GLUT4 antibody, and blotted with anti-GPC3 antibody. In adipocytes, we detected the interaction between GLUT4 and non-glycosylated GPC3 core protein (Fig. 3A). We also confirmed these interactions by immunoprecipitation with anti-GPC3 antibody (Fig. 3B). Second, we assessed the direct interaction between GLUT4 and GPC3 using the GST pull-down assay. We generated GST-GPC3 protein and GST alone using a bacterial system, and then purified these proteins with glutathione–sepharose beads. GLUT4 protein was purified from 293 cells transfected with 4×Myc-tagged-GLUT4-eGFP. These fusion proteins were mixed in PBS, and incubated for several hours. The proteins were then pulled down with glutathione–sepharose beads. We confirmed the GLUT4 signal in the GST-GPC3 precipitate lane, indicating a direct GLUT4 and GPC3 interaction in vitro (Fig. 3C).

*Overexpression of GPC3 increased insulin stimulated glucose uptake*

Since GPC3 was proved to GLUT4 at the plasma membrane, we examined whether GPC3 might regulate glucose uptake through GLUT4. We measured basal and insulin stimulated glucose uptake in 3T3-L1 adipocytes which transiently overexpressed GPC3 following transfection with adenovirus vectors. Overexpression of GPC3 increased insulin induced glucose uptake (Fig. 4). These data suggested that GPC3 overexpression to enhance insulin-stimulated glucose uptake via cell surface GLUT4.

Simpson–Golabi–Behmel syndrome (SGBS) is a rare, complex congenital syndrome with affected individuals having loss of function mutations in the GPC3 gene. Although many researchers

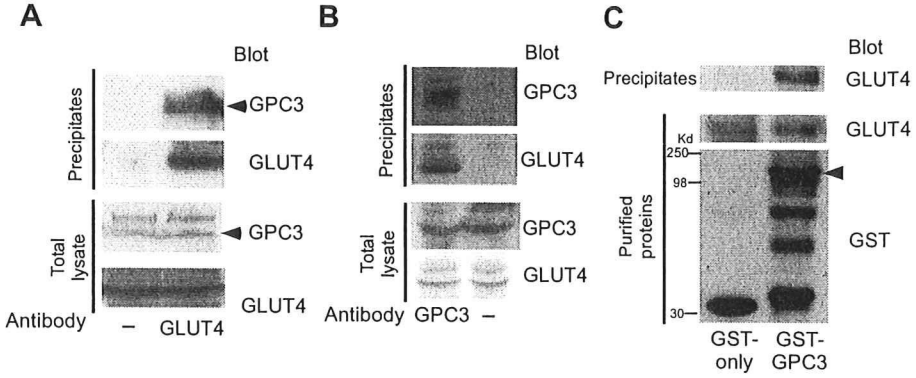


**Fig. 3.** GPC3 binds to GLUT4. (A) 3T3-L1 adipocytes were stimulated with 100 nM of insulin for 15 min. The lysates were incubated with or without anti-GLUT4 rabbit antibody followed by precipitation with protein A sepharose beads. Precipitates were separated by SDS–PAGE and immunoblotted with anti-GPC3 mouse monoclonal and anti-GLUT4 goat antibodies. Protein signals were visualized using horseradish peroxidase-conjugated secondary antibodies and an enhanced chemiluminescence substrate kit (GE Healthcare Biosciences). Arrowhead indicates GPC3 core protein. (B) 3T3-L1 adipocytes were stimulated with 100 nM of insulin for 15 min. Then, lysates of these adipocytes were immunoprecipitated using anti-GPC3 antibody or beads only. Precipitates were immunoblotted with anti-GLUT4 and anti-GPC3 antibodies for determination of GPC3-binding proteins. (C) GST-GPC3 and GST alone were bacterially expressed and purified by glutathione–sepharose beads. 4×Myc-tagged GLUT4-eGFP protein was expressed in 293 cells and purified using anti-Myc antibodies. Purified GST-GPC3 or GST proteins and GLUT4 protein were mixed and pulled down with glutathione–sepharose beads. The precipitates were separated by SDS–PAGE and analyzed by Western blotting using anti-GLUT4 and anti-GST antibodies. Arrowhead indicates full-length GST-GPC3.

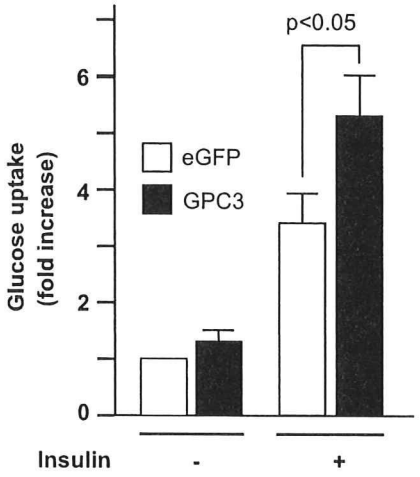


**Fig. 4.** Effect of GPC3 expression on glucose uptake 3T3-L1 adipocytes were infected with recombinant adenovirus vectors encoding FLAG-GPC3 or eGFP as a control at a m.o.i. of 50. The cells were serum-starved for 3 h and treated with or without 100 nM of insulin for 15 min. Glucose uptake was determined by 2-deoxy-D-[2,6$^3$H] glucose incorporation. Non-specific glucose uptake was measured in the presence of 20 μM cytochalasin B and subtracted from each determination to obtain the specific uptake. Statistical analyses were performed using Student's *t*-test. Experiments were repeated six times. Values are expressed as means ± SE, as indicated.

reported that the patients have general feature of overgrowth and cancer development, little is known about the clinical characteristics on glucose metabolism [18–21]. It was reported that some infants had hypoglycemia due to hyperplasia of islets of Langerhans rather than modification of insulin action in peripheral tissues [22]. More detailed analysis for the peripheral insulin action, especially on the adipose tissue would clarify the physiological role of GPC3 on glucose metabolism.

In conclusion, we identified a novel GLUT4-binding protein GPC3, using a yeast two-hybrid screening system. We also demonstrated GPC3 and GLUT4 to co-localized at the plasma membrane in response to insulin. Furthermore, overexpression of GPC3 increased insulin stimulated glucose uptake in cultured adipocytes. GPC3 may play a role in insulin stimulated glucose uptake.

## Acknowledgments

We are also very grateful to Dr. Teruo Nishida for generously supporting us in the using a laser confocal microscope experiments. The authors thank Y. Kora and M. Kaneko for technical assistance. This study was supported in part by Grants-in-Aid for Scientific Research (17590934 to M. Emoto, 15590939 and 17590935 to S. Okuya) from the Ministry of Education, Culture, Sports, Science and Technology of Japan, and a grant from Takeda Science Foundation to S. Okuya.

## References

[1] J.C. Hou, J.E. Pessin, Ins (endocytosis) and outs (exocytosis) of GLUT4 trafficking, Curr. Opin. Cell Biol. 19 (2007) 466–473.
[2] S. Huang, M.P. Czech, The GLUT4 glucose transporter, Cell Metab. 5 (2007) 237–252.
[3] F. Giorgino, O. de Robertis, L. Laviola, C. Montrone, S. Perrini, K.C. McCowen, R.J. Smith, The sentrin-conjugating enzyme mUbc9 interacts with GLUT4 and GLUT1 glucose transporters and regulates transporter levels in skeletal muscle cells, Proc. Natl. Acad. Sci. USA 97 (2000) 1125–1130.
[4] J.S. Bogan, N. Hendon, A.E. McKee, T.S. Tsao, H.F. Lodish, Functional cloning of TUG as a regulator of GLUT4 glucose transporter trafficking, Nature 425 (2003) 727–733.
[5] V.S. Lalioti, S. Vergarajauregui, D. Pulido, I.V. Sandoval, The insulin-sensitive glucose transporter, GLUT4, interacts physically with Daxx. Two proteins with capacity to bind Ubc9 and conjugated to SUMO1, J. Biol. Chem. 277 (2002) 19783–19791.
[6] Y. Shi, S.J. Samuel, W. Lee, C. Yu, W. Zhang, M. Lachaal, C.Y. Jung, Cloning of an L-3-hydroxyacyl-CoA dehydrogenase that interacts with the GLUT4 C-terminus, Arch. Biochem. Biophys. 363 (1999) 323–332.
[7] W. Lee, J. Ryu, J. Hah, T. Tsujita, C.Y. Jung, Association of carboxyl esterase with facilitative glucose transporter isoform 4 (GLUT4) intracellular compartments in rat adipocytes and its possible role in insulin-induced GLUT4 recruitment, J. Biol. Chem. 275 (2000) 10041–10046.
[8] J. Filmus, Glypicans in growth control and cancer, Glycobiology 11 (2001) 19R–23R.
[9] D.F. Cano-Gauci, H.H. Song, H. Yang, C. McKerlie, B. Choo, W. Shi, R. Pullano, T.D. Piscione, S. Grisaru, S. Soon, L. Sedlackova, A.K. Tanswell, T.W. Mak, H. Yeger, G.A. Lockwood, N.D. Rosenblum, J. Filmus, Glypican-3-deficient mice exhibit developmental overgrowth and some of the abnormalities typical of Simpson–Golabi–Behmel syndrome, J. Cell Biol. 146 (1999) 255–264.
[10] H. Lin, R. Huber, D. Schlessinger, P.J. Morin, Frequent silencing of the GPC3 gene in ovarian cancer cell lines, Cancer Res. 59 (1999) 807–810.
[11] Y. Midorikawa, S. Ishikawa, H. Iwanari, T. Imamura, H. Sakamoto, K. Miyazono, T. Kodama, M. Makuuchi, H. Aburatani, Glypican-3, overexpressed in hepatocellular carcinoma, modulates FGF2 and BMP-7 signaling, Int. J. Cancer 103 (2003) 455–465.
[12] H.H. Song, W. Shi, Y.Y. Xiang, J. Filmus, The loss of glypican-3 induces alterations in Wnt signaling, J. Biol. Chem. 280 (2005) 2116–2125.

[13] M.I. Capurro, W. Shi, S. Sandal, J. Filmus, Processing by convertases is not required for glypican-3-induced stimulation of hepatocellular carcinoma growth, J. Biol. Chem. 280 (2005) 41201–41206.
[14] J.D. Horton, H. Shimano, R.L. Hamilton, M.S. Brown, J.L. Goldstein, Disruption of LDL receptor gene in transgenic SREBP-1a mice unmasks hyperlipidemia resulting from production of lipid-rich VLDL, J. Clin. Invest. 103 (1999) 1067–1076.
[15] M. Emoto, S.E. Langille, M.P. Czech, A role for kinesin in insulin-stimulated GLUT4 glucose transporter translocation in 3T3-L1 adipocytes, J. Biol. Chem. 276 (2001) 10677–10682.
[16] J. Filmus, J.G. Church, R.N. Buick, Isolation of a cDNA corresponding to a developmentally regulated transcript in rat intestine, Mol. Cell. Biol. 8 (1988) 4243–4249.
[17] K. Watanabe, H. Yamada, Y. Yamaguchi, K-Glypican: a novel GPI-anchored heparan sulfate proteoglycan that is highly expressed in developing brain and kidney, J. Cell Biol. 130 (1995) 1207–1218.
[18] G. Pilia, R.M. Hughes-Benzie, A. MacKenzie, P. Baybayan, E.Y. Chen, R. Huber, G. Neri, A. Cao, A. Forabosco, D. Schlessinger, Mutations in GPC3, a glypican gene, cause the Simpson–Golabi–Behmel overgrowth syndrome, Nat. Genet. 12 (1996) 241–247.
[19] N. Okamoto, M. Yagi, K. Imura, Y. Wada, A clinical and molecular study of a patient with Simpson–Golabi–Behmel syndrome, J. Hum. Genet. 44 (1999) 327–329.
[20] S. Lindsay, M. Ireland, O. O'Brien, J. Clayton-Smith, J.A. Hurst, J. Mann, T. Cole, J. Sampson, S. Slaney, D. Schlessinger, J. Burn, G. Pilia, Large scale deletions in the GPC3 gene may account for a minority of cases of Simpson–Golabi–Behmel syndrome, J. Med. Genet. 34 (1997) 480–483.
[21] J.Y. Xuan, A. Besner, M. Ireland, R.M. Hughes-Benzie, A.E. MacKenzie, Mapping of Simpson–Golabi–Behmel syndrome to Xq25–q27, Hum. Mol. Genet. 3 (1994) 133–137.
[22] M.R. DeBaun, J. Ess, S. Saunders, Simpson–Golabi–Behmel syndrome: progress toward understanding the molecular basis for overgrowth, malformation, and cancer predisposition, Mol. Genet. Metab. 72 (2001) 279–286.

Available online at www.sciencedirect.com
ScienceDirect
Developmental Biology 313 (2008) 335–346
DEVELOPMENTAL BIOLOGY
www.elsevier.com/developmentalbiology

# Maintenance of genomic methylation patterns during preimplantation development requires the somatic form of DNA methyltransferase 1

Yukiko Kurihara [a,*], Yumiko Kawamura [a], Yasunobu Uchijima [a], Tomokazu Amamo [b], Hiroshi Kobayashi [a], Tomoichiro Asano [a,c], Hiroki Kurihara [a]

[a] *Department of Physiological Chemistry and Metabolism, Graduate School of Medicine, The University of Tokyo, 7-3-1 Hongo, Bunkyo-ku, Tokyo 113-0033, Japan*
[b] *Department of Developmental Medical Technology (Sankyo), Graduate School of Medicine, The University of Tokyo, Tokyo 113-0033, Japan*
[c] *Department of Biomedical Chemistry, Hiroshima University Graduate School of Biomedical Sciences, Hiroshima 734-8551, Japan*

Received for publication 27 April 2007; revised 17 October 2007; accepted 22 October 2007
Available online 30 October 2007

**Abstract**

DNA methylation at cytosine residues in CpG dinucleotides is a component of epigenetic marks crucial to mammalian development. In preimplantation stage embryos, a large part of genomic DNA is extensively demethylated, whereas the methylation patterns are faithfully maintained in certain regions. To date, no enzymes responsible for the maintenance of DNA methylation during preimplantation development have been identified except for the oocyte form of DNA (cytosine-5)-methyltransferase 1 (Dnmt1o) at the 8-cell stage. Herein, we demonstrate that the somatic form of Dnmt1 (Dnmt1s) is present in association with chromatin in MII-stage oocytes as well as in the nucleus throughout preimplantation development. At the early one-cell stage, Dnmt1s is asymmetrically localized in the maternal pronuclei. Thereafter, Dnmt1s is recruited to the paternal genome during pronuclear maturation. During the first two cell cycles after fertilization, Dnmt1s is exported from the nucleus in the G2 phase in a CRM1/exportin-dependent manner. Antibody microinjection and small interfering RNA-mediated knock-down decreases methylated CpG dinucleotides in repetitive intracisternal A-type particle (IAP) sequences and the imprinted gene *H19*. These results indicate that Dnmt1s is responsible for the maintenance methylation of particular genomic regions whose methylation patterns must be faithfully maintained during preimplantation development.


*Keywords:* DNA methylation; DNA methyltransferase; Preimplantation development; Genomic imprinting; Nucleocytoplasmic shuttling

## Introduction

DNA methylation at cytosine residues in CpG dinucleotides is a component of epigenetic marks crucial to mammalian development (Jaenisch and Bird, 2003; Li, 2002; Reik et al., 2001). After fertilization, the zygote undergoes extensive demethylation of genomic DNA (Dean et al., 2003; Morgan et al., 2005; Santos and Dean, 2004). Genomic DNA of paternal origin is actively demethylated within several hours after fertilization, whereas the oocyte-derived maternal genome is thought to be passively demethylated, resulting in a parental asymmetry in epigenetic marks (Mayer et al., 2000; Oswald et al., 2000; Rougier et al., 1998). *De novo* and maintenance DNA methylation throughout the genome is restored around the time of implantation to establish tissue-specific epigenetic states. As for germline development, highly methylated primordial germ cells migrate to the genital ridge and then undergo loss and reacquisition of methylation. Thus, two rounds of demethylation/remethylation events constitute an epigenetic cycle in mammals.

Contrary to the genome-wide loss of DNA methylation, methylation states of certain sequences are well preserved during preimplantation development. For example, the monoallelic methylation of imprinted genes such as *H19* and *Snrpn* must be faithfully maintained for normal development (Doherty et al., 2002; Tremblay et al., 1997; Warnecke et al., 1998). The intracisternal A-type particle (IAP), a repetitive sequence of retrotransposon, is also resistant to demethylation in preim-

* Corresponding author. Fax: +81 3 5684 4958.
*E-mail address:* yuki-tky@umin.net (Y. Kurihara).

0012-1606/$ - see front matter © 2007 Elsevier Inc. All rights reserved.
doi:10.1016/j.ydbio.2007.10.033

plantation embryos (Gaudet et al., 2004; Lane et al., 2003). The methylation of these genes is important for preventing their deregulated activation, which may lead to deleterious consequences such as growth abnormalities and tumorigenesis (Egger et al., 2004; Yoder et al., 1997). However, the mechanism distinguishing methyl-CpG-containing sequences to be demethylated versus those to be maintained in preimplantation embryos remains unknown.

Three enzymes with DNA (cytosine-5)-methyltransferase (Dnmt) activity have been identified in mammals (Bestor, 2000). Dnmt1, a large protein with a molecular mass of 190 kDa, predominantly catalyzes maintenance methylation via binding to proliferating cell nuclear antigen (PCNA) in replication foci during the S phase (Bestor et al., 1988; Chuang et al., 1997; Leonhardt et al., 1992). Two other enzymes, Dnmt3a and Dnmt3b, are mainly responsible for *de novo* methylation that establishes a new DNA methylation state (Okano et al., 1999, 1998). Inactivation of both Dnmt3a and Dnmt3b results in defective *de novo* methylation in embryonic stem cells and early embryos but has no discernable effect on the maintenance of preexisting methylation patterns in postimplantation embryos, indicating that virtually all DNA methylation is maintained by Dnmt1 during postimplantation development (Li et al., 1992; Okano et al., 1999).

Unfertilized oocytes and preimplantation embryos are characterized by the presence of Dnmt1o, an isoform of Dnmt1 (Mertineit et al., 1998). Dnmt1o is distinct from the conventional Dnmt1 expressed in most somatic cells (Dnmt1s) in that it uses the oocyte-specific 5′ exon, resulting in the formation of an N-terminally truncated protein with a molecular mass of 175 kDa (Mertineit et al., 1998). During preimplantation development, Dnmt1o protein is translated from oocyte-derived mRNA and is actively retained in the cytoplasm except at the eight-cell stage, when Dnmt1o is transiently translocated to the nucleus (Cardoso and Leonhardt, 1999; Doherty et al., 2002; Howell et al., 2001; Mertineit et al., 1998; Ratnam et al., 2002) Mice homozygous for the Dnm1o-specific knockout allele were normal, but most heterozygotes from homozygous females were embryonic lethal with a partial loss of methylation at imprinted loci (Howell et al., 2001). In contrast, no Dnmt1s protein has been detected in oocytes and preimplantation embryos, although its transcripts are present (Cardoso and Leonhardt, 1999; Ratnam et al., 2002). These findings have led to the conclusion that Dnmt1o is the only known form of maintenance methyltransferase present in preimplantation embryos and that, except at the eight-cell stage, methylation patterns must be maintained by as yet unknown enzymes (Howell et al., 2001; Ratnam et al., 2002).

Here we demonstrate that Dnmt1s protein is present during preimplantation development. Characteristically, the nuclear localization in 1- and 2-cell stage embryos appears to be controlled by a CRM1/exportin-mediated nucleocytoplasmic shuttling. Furthermore, inactivation of Dnmt1s in preimplantation embryos revealed that it functions as a maintenance DNA methyltransferase for certain genomic regions including imprinted and repetitive genes.

## Materials and methods

### *Collection of oocytes and embryos*

Female ICR mice (8–10 weeks old) were superovulated with intraperitoneal injections of 5 IU of pregnant mare serum gonadotropin (PMSG; Teikoku Hormone Mfg.) and, 48 h later, 5 IU of human chorionic gonadotropin (hCG; Teikoku Hormone Mfg.). Oocytes were recovered from the oviducts 20 h after hCG injection, and cumulus cells were extensively dispersed with 1 mg/ml hyaluronidase (Sigma). Preimplantation embryos were obtained from superovulated females mated to ICR males on appropriate days for each cleavage stage. To obtain one-cell embryos at early pronuclear stages, ICSI or *in vitro* fertilization (IVF) was performed on unfertilized oocytes collected as above and sperm obtained from ICR males according to standard procedures. Embryos were cultured in KSOM medium at 37 °C in humidified air containing 5% $CO_2$.

### *Plasmids*

The mouse Dnmt1s cDNA was cloned by RT-PCR on total RNA from the mouse liver. For glutathione *S*-transferase (GST) fusion protein, a cDNA fragment encoding the N-terminal 118 amino acids of Dnmt1s was subcloned in-frame into the pGEX vector (Amersham Pharmacia Biotech). For a series of enhanced green fluorescence protein (EGFP)-fusion constructs, cDNA fragments encompassing the open reading frame of Dnmt1s and its derivatives were subcloned in-frame into the pEGFP-C2 expression vector (Clontech). Fragments encoding EGFP-Dnmt1 constructs were then subcloned into pBluescript (Stratagene) or pCRII-TOPO (Invitrogen) for *in vitro* transcription. All the constructs were verified by sequencing.

### *Antibodies*

To generate polyclonal antibody against the N-terminal region of Dnmt1s, we prepared fusion proteins between GST and the N-terminal 118 amino acids of Dnmt1s in *Escherichia coli*, and purified them using glutathione-coupled Sepharose beads. The purified GST fusion proteins were injected into rabbits. The antibody, named N48, was affinity-purified using this antigen bound to Affi-Gel 10 (Bio-Rad).

### *Cell culture and transfection*

NIH3T3 cells were cultured in Dulbecco's modified Eagle's medium containing 10% fetal calf serum and antibiotics at 37 °C in 5% $CO_2$. For transfection of small interfering RNA (siRNA), cells were grown to 50–90% confluence and were treated with mixture of siRNA and OligofectAMINE reagents (Invitrogen) according to the manufacturer's protocol.

### *Western blotting*

A pool of ~500 unfertilized oocytes were lysed in PBS containing 1% Nonidet P-40 and protease inhibitors, and then subjected to 7.5% SDS-PAGE with lysates of NIH3T3 cells. The separated proteins were transferred to a nylon membrane, which was then pre-treated with 3% bovine serum albumin for blocking and incubated with the N48 antibody and treated with anti-rabbit IgG antibody conjugated to horseradish peroxidase (ICN). The protein bands were visualized using an ECL Plus Western Blotting Detection System (Amersham Pharmacia Biotech). Then, the membrane was washed and re-blotted with the H-300 antibody recognizing the C-terminus of Dnmt1 (rabbit, Santa Cruz). The relative amounts of proteins were estimated by densitometry using the ImageJ software (NIH).

### *Immunostaining*

Unfertilized oocytes and preimplantation embryos were freed of the zona pellucida by using acidified Tyrode's medium, fixed for 15 min in 4%

paraformaldehyde in PBS, and permeabilized with 0.2% Triton X-100 in PBS for 5 min at room temperature. After blocking for 30 min in 5% normal donkey serum, the samples were incubated in the same solution with the N48 or H-300 antibodies overnight at 4°C. Then, the samples were washed and stained with the secondary antibodies (FITC- or rhodamine-conjugated donkey anti-rabbit IgG (Jackson Immunoresearch). Staining with rabbit polyclonal anti-GFP antibody (MBL) served as negative control. DNA was visualized by staining with DAPI (1μg/ml) or propidium iodide (50μg/ml). Confocal images were obtained using a Nikon D-ECLIPSE C1 system.

For semi-quantitative analysis of immunofluorescent signals, the pixel value/unit was measured for the nuclear and cytoplasmic signals using ImageJ software (NIH) and the relative nuclear intensity was evaluated by dividing the pixel value/unit of the nuclear signal by that of the cytoplasmic signal. Data were analyzed using analysis of variance (ANOVA) and significance was defined as $P<0.05$ (Sheffe's $F$-test).

### *RNA preparation and microinjection*

Preparation and injection of *in vitro* transcribed mRNA were performed as previously described (Aida et al., 2001). Briefly, plasmids containing EGFP-Dnmt1 fusion constructs were linearized and used as templates for *in vitro* transcription employing the T7 MessageMachine kit (Ambion). Synthesized RNA was further polyadenylated by yeast poly(A) polymerase (Amersham Biosciences) and resolved in 150 mM KCl with a final concentration of ~100 ng/μl. The diluted RNA was filtered, heated at 90 °C for 1 min and cooled on ice. Then, ~10 pl of the RNA solution were injected into fertilized eggs or two-cell embryos through a glass micropipette. Fluorescent images were obtained and the relative nuclear intensity was evaluated as in the case of immunostaining.

### *ICSI with microinjection of antibodies*

ICSI was performed as previously described (Kimura and Yanagimachi, 1995). Antibodies were premixed in the sperm suspension to be introduced into oocytes. Anti-GST antibody served as a negative control.

### *RNA interference*

Chemically synthesized 27-nt siRNA duplexes with no overhang were commercially obtained (Japan Bio-Service). Two different sequences for Dnmt1s were selected for the generation of siRNA; the sequences for si290 and si322 corresponded to nucleotides 290–316 and 322–348 of mouse Dnmt1s (GenBank accession number NM_010066), respectively. Inv322, a siRNA possessing the inverted sequence of si322, served as a control. Approximately 10 pl of 20 μM siRNA were injected into the cytoplasm of unfertilized eggs, which were subsequently subjected to *in vitro* fertilization.

### *DNA methylation analysis*

About 20–40 embryos were embedded in one agarose droplet, which was then treated with sodium bisulfite for cytosine modification as described (Olek et al., 1996). Each sample was subdivided into 2–3 tubes and was subjected to two-round nested PCR analysis. PCR primers were synthesized to analyze the methylation status of the *H19* upstream DMD (GenBank accession number U19619, nucleotides 1304–1726) (Tremblay et al., 1997) and the LTR of IAP (GenBank accession number M17551, nucleotides 48–305) (Lane et al., 2003). Amplified PCR products were subcloned into PCRII-TOPO vector and were sequenced. Bisulfite reaction was considered complete when more than 99% of the cytosines were converted to thymines. For IAP, 3–5 clones were sequenced from each PCR template. For *H19*, paternal alleles were distinguished by a single polymorphism in the analyzed region (Tremblay et al., 1997) and one representative sequence (the youngest number of several sequenced clones) was adopted from each template. Primer sequences are available on request.

Statistical analysis was performed by Mann–Whitney's $U$-test for two-group comparison of antibody-injected embryos, and by one-way ANOVA, Sheffe's post hoc analysis for three-group comparison of siRNA-injected embryos. $P$ values less than 0.05 were considered significant.

## Results

### *Dnmt1s protein is present in mouse unfertilized oocytes and preimplantation embryos*

To test the current assumption that Dnmt1s mRNA is not translated into proteins during preimplantation development, we first raised a rabbit polyclonal antibody against the N-terminal region specific for the Dnmt1s isoform (Fig. 1A). This antibody, named N48, was capable of detecting a single band with a molecular mass of ~190 kDa in Western blot of MII-stage unfertilized oocyte extracts as well as NIH3T3 cell extracts (Fig. 1B). For comparison, the membrane was re-probed with H-300, an antibody recognizing the C-terminal region of both Dnmt1s and Dnmt1o. Signal intensity was adjusted by changing blotting condition and exposure times to allow comparison of the amounts of Dnmt1s and Dnmt1o as below. As expected, H-300 detected ~175-kDa Dnmt1o in unfertilized oocytes and ~190 kDa-Dnmt1s in NIH3T3 cells (Fig. 1B). Using the signal intensities from different volumes (1× and 4×) of NIH3T3 extracts as references, Dnmt1s was estimated to be ~2000-fold less abundant than Dnmt1o in MII-stage unfertilized oocytes. The presence of Dnmt1s was also confirmed with another Dnmt1s-specific antibody UPT82 (Ratnam et al., 2002) (data not shown). Dnmt1s was also detected in morula-stage embryos by both N48 and UPT82 antibodies (data not shown).

To determine the localization of Dnmt1s, MII-stage unfertilized oocytes were stained with the N48 antibody. In contrast to the cytoplasmic distribution of Dnmt1o as shown by staining with H-300, Dnmt1s signals were exclusively localized to meiotic chromosomes (Fig. 1C). After fertilization, growing preimplantation embryos showed the presence of Dnmt1s in the nucleus until the blastocyst stage, whereas Dnmt1o signals were predominantly detected in the cytoplasm (Fig. 1D). Although previous reports showed nuclear translocation of Dnmt1o at the 8-cell stage (Doherty et al., 2002; Howell et al., 2001), H-300 antibody detected only weakly the nuclear Dnmt1o possibly due to differences in epitope recognition. These results indicate that Dnmt1s proteins are translated and localized to the nucleus during preimplantation development, whereas Dnmt1o reciprocally distributes throughout the cytoplasm.

### *Differential localization of Dnmt1s between paternal and maternal pronuclei*

To investigate the dynamics of Dnmt1s localization from fertilization to the first cleavage, mouse one-cell embryos were collected 2 and 5 h after intracytoplasmic sperm injection (ICSI), and 21, 27 and 30 h after hCG injection with natural crossbreeding. Embryos were then stained with N48 antibody and propidium iodide (PI). According to the size and location of the pronuclei in the cytoplasm, samples were assigned to one of the pronuclear stages, PN0–PN5 (Adenot et al., 1997; Santos et al., 2002). Each sampling time approximately corresponded to PN0, PN1–2, PN3–4, PN5 and M-phase, respectively.

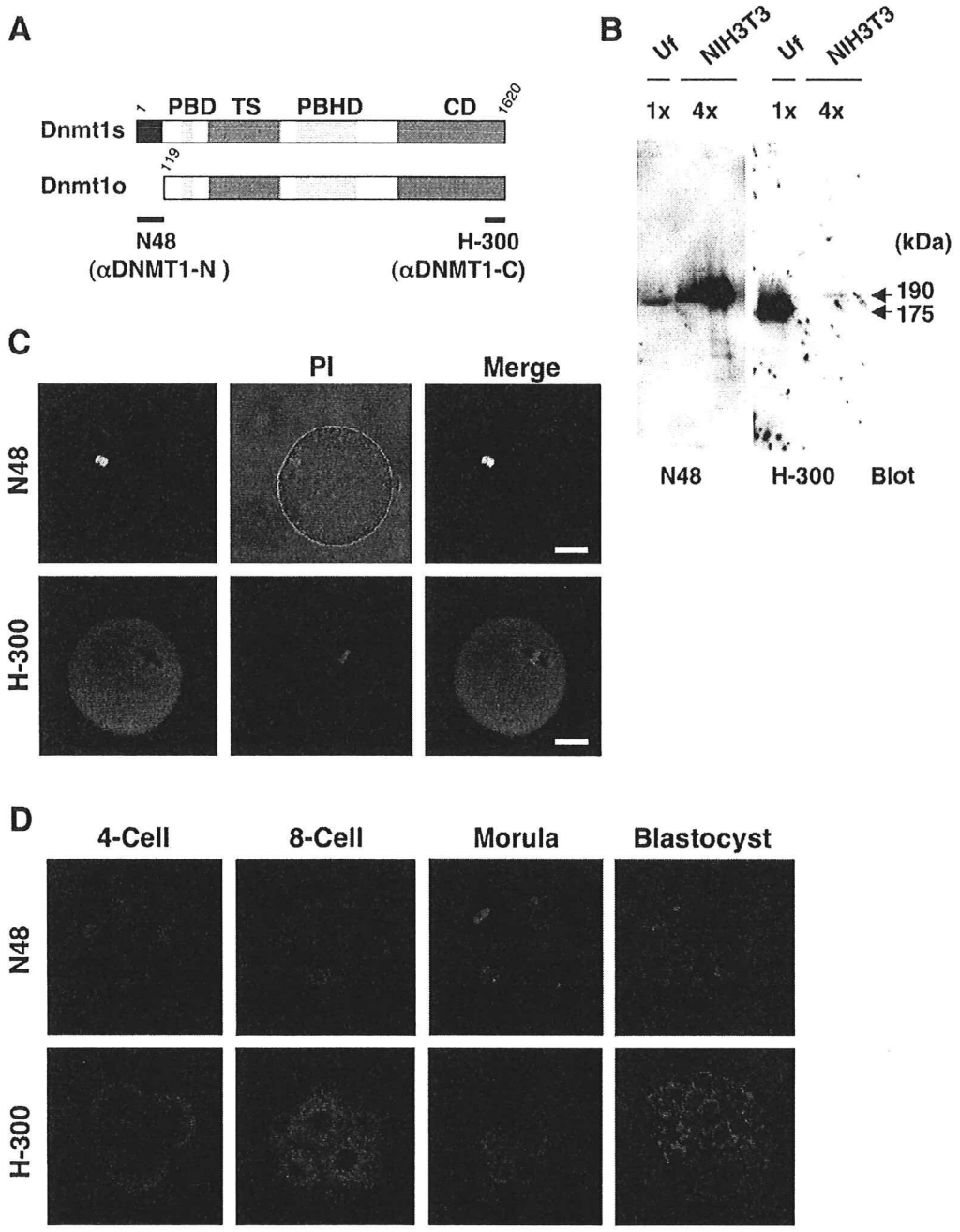


Fig. 1. Presence and localization of Dnmt1s in mouse unfertilized eggs and preimplantation embryos. (A) Structures of Dnmt1 isoforms and locations of epitopes recognized by two different antibodies; N48 and H-300. PBD, PCNA binding domain; TS, DNA replication foci-targeting sequence; PBHD, polybromo homology domain; CD, catalytic domain. (B) Western blotting of extracts from mouse unfertilized eggs (Uf) and NIH3T3 cells, probed with N48 and then reprobed with H-300. N48 detected only the 190 kDa Dnmt1s, whereas H-300 detected both 190 kDa Dnmt1s and 175 kDa Dnmt1o. Signals from different volumes (1× and 4×) of NIH3T3 extracts were used for comparison of relative amounts of Dnmt1 isoforms. (C) Immunostaining of mouse MII-stage unfertilized eggs with N48 and H-300. DNA was visualized by PI staining. For staining with N48 and PI, the PI staining image was superimposed on the corresponding light microscopic image. Dnmt1s colocalizes with meiotic chromosomes, as seen in yellow (merged image), whereas Dnmt1o distributes reciprocally in the cytoplasm. Scale bars indicate 20 μm. (D) Immunostaining of mouse preimplantation embryos. Dnmt1s is detected in the nuclei, whereas Dnmt1o is predominantly distributed in the cytoplasm.

At PN0, the fertilizing sperm is decondensed and the second polar body is eliminated upon the completion of meiosis. At this stage, Dnmt1s was exclusively detected in association with the maternal genome (Fig. 2A). As maturation of the pronuclei proceeded from PN1 to PN4, faint Dnmt1s signals also appeared in the paternal pronucleus, although at lower intensity than that of the maternal pronucleus (Figs. 2B, C). In three embryos at PN3–4, intense Dnmt1s signals were detected in the paternal pronucleus in a punctate pattern (Fig. 2D). These findings indicate that Dnmt1s is recruited to the paternal

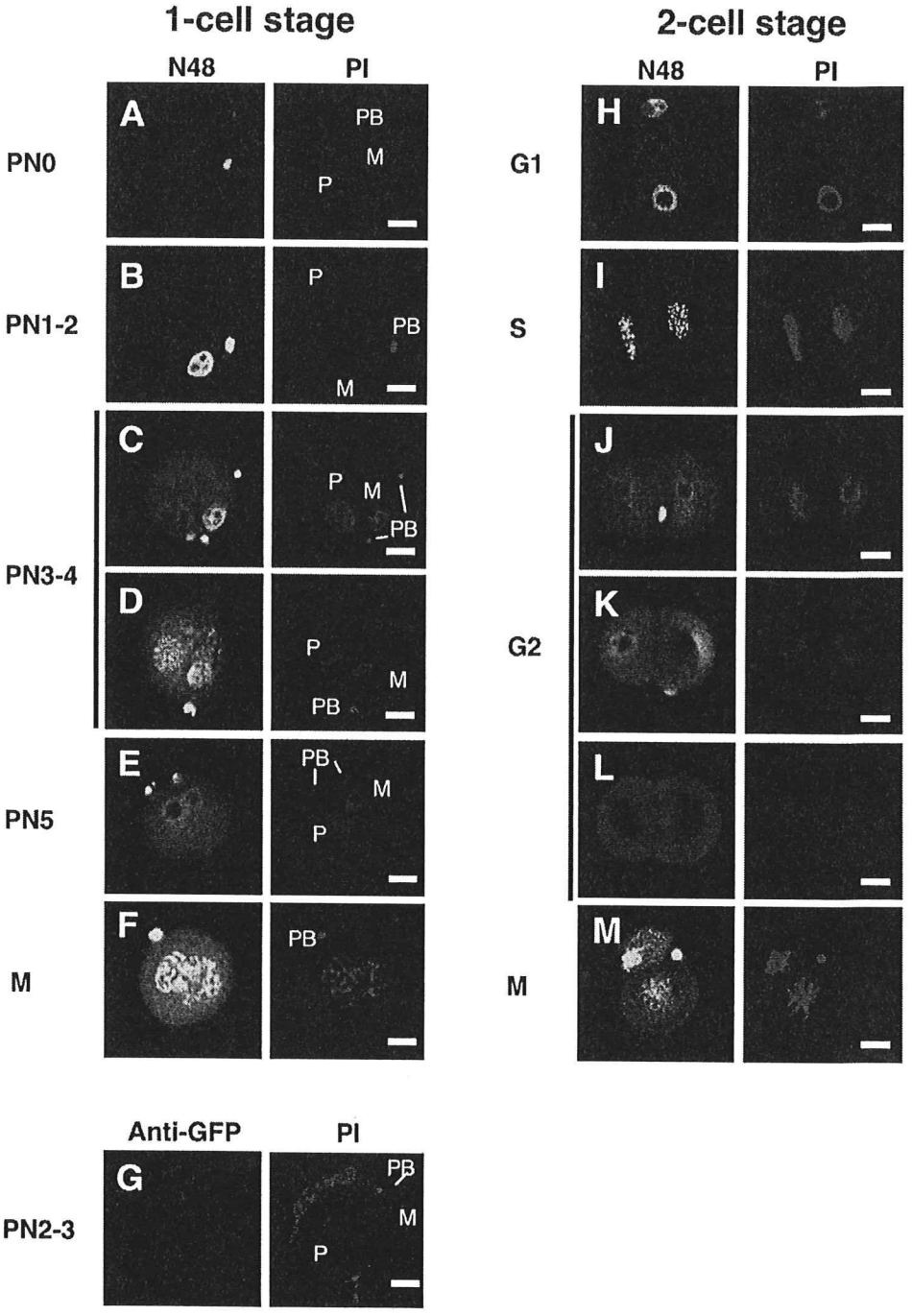


Fig. 2. Localization of Dnmt1s in one- and two-cell stage embryos. (A–F) Representative immunofluorescent images of one-cell embryos stained with the N48 antibody at different pronuclear stages. DNA was visualized by PI staining. The identity of the pronuclei was determined by their size and position relative to the polar body. At PN0, Dnmt1s is detected only in association with the maternal genome (A). Dnmt1s is thereafter localized predominantly in the maternal pronucleus until PN5 (B–D). Dnmt1 is also detected in the paternal nucleus, but the signals are quite faint (B, C). At PN3–4, some embryos show intense Dnmt1s signals in the paternal pronucleus in a punctate pattern (D). At PN5, Dnmt1s largely disappears from the pronuclei (E). At syngamy, Dnmt1 again colocalizes to the chromosome (F). (G) Control staining with anti-GFP antibody. (H–M) Representative immunofluorescent images of two-cell embryos stained with the N48 antibody at different cell cycle phases. Dnmt1 localizes in the nucleus through the G1 (H) to the S phase (I). Dnmt1s signals in the S phase show a punctate pattern. Then, Dnmt1s in the nucleus was largely decreased in the G2 phase (J). In some cases, Dnmt1s signals were absent from the nucleus in either (K) or both (L) of the blastomeres in G2. In the M phase, Dnmt1 again localizes in close association with the chromosomes (M). M, maternal pronucleus; P, paternal pronucleus; PB, polar body. Scale bars indicate 20 μm.

genome during pronuclear maturation with a peak during PN3–4. At PN5, Dnmt1s signals in the maternal pronucleus were reduced to the paternal pronucleus level (Fig. 2E). During mitosis, Dnmt1s again colocalized intensely to the chromosomes (Fig. 2F). Staining with anti-GFP antibody as negative control gave little signals (Fig. 2G).

*Dynamic changes in nuclear localization of Dnmt1s in early preimplantation embryos*

In addition to asymmetric localization of Dnmt1s in the pronuclei, immunostaining analysis revealed dynamic changes in this protein during pronuclear maturation through to the first cleavage. The pronuclear staging has been shown to correlate with cell cycle phases; PN1–2 embryos are in G1, PN3–4 embryos are largely in S, and PN5 embryos are mostly in G2 (Adenot et al., 1997). Significantly, the punctate pattern of Dnmt1s signals in PN3–4 embryos is very similar to that associated with the DNA replication foci in cultured somatic cells in middle and late S phase (Leonhardt et al., 1992; Liu et al., 1998). Therefore, the dynamics of localization in one-cell embryos suggest that Dnmt1 may be recruited and sustained in the pronucleus during the G1 to S phases, and then excluded from the pronucleus in the G2 phase. To test this possibility at later stages, we examined the dynamics of Dnmt1s localization in two-cell embryos.

It has been reported that, during the second cell cycle, the G1, S and G2 phases last about 2, 6–7 and 14 h, respectively (Moore et al., 1996). On the basis of this report, two-cell embryos were collected 1 h (G1), 6 h (S) and 12–20 h (G2) after the first cleavage and stained with N48 antibody and PI. Dnmt1s was diffusely distributed in the nucleoplasm in the G1 phase (Fig. 2H). In the S phase, Dnmt1s signals showed a punctate pattern in the nucleus (Fig. 2I), as seen in somatic cells in the same phase. In contrast, many embryos exhibited significantly reduced Dnmt1s signals in the nucleus during the G2 phase (Fig. 2J). In some cases, Dnmt1s signals were absent from the nucleus in either or both of the blastomeres (Figs. 2K, L), indicating the transient disappearance of Dnmt1s from the nucleus during the G2 phase. During mitosis, Dnmt1s was

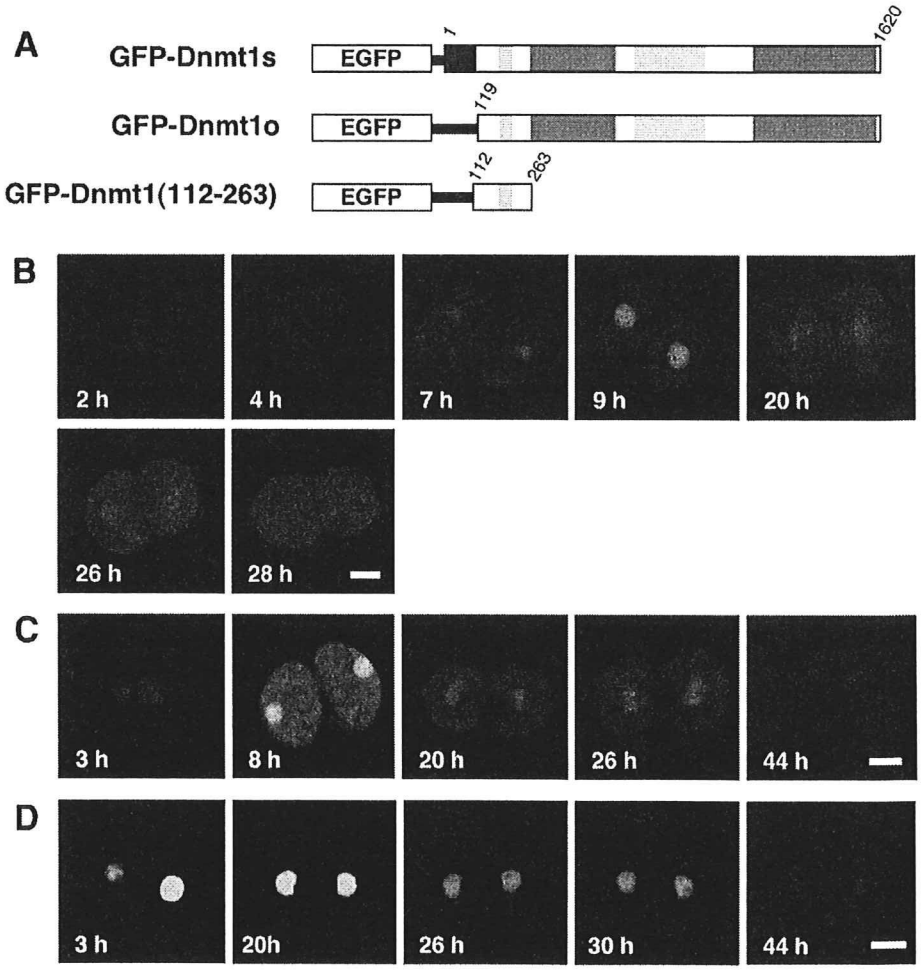


Fig. 3. Dynamic changes in the localization of EGFP-Dnmt1 mutant proteins. (A) Structures of EGFP-Dnmt1 mutant proteins. (B–D) *In vitro* transcripts for EGFP-Dnmt1s (B), EGFP-Dnmt1o (C) and EGFP-Dnmt1(112–263) (D) were microinjected into one-cell embryos and fluorescent images were serially obtained by confocal microscopy. Shown are representative embryos expressing each EGFP-Dnmt1 mutant protein. Time is in hours after mRNA injection. Scale bars indicate 20 μm.

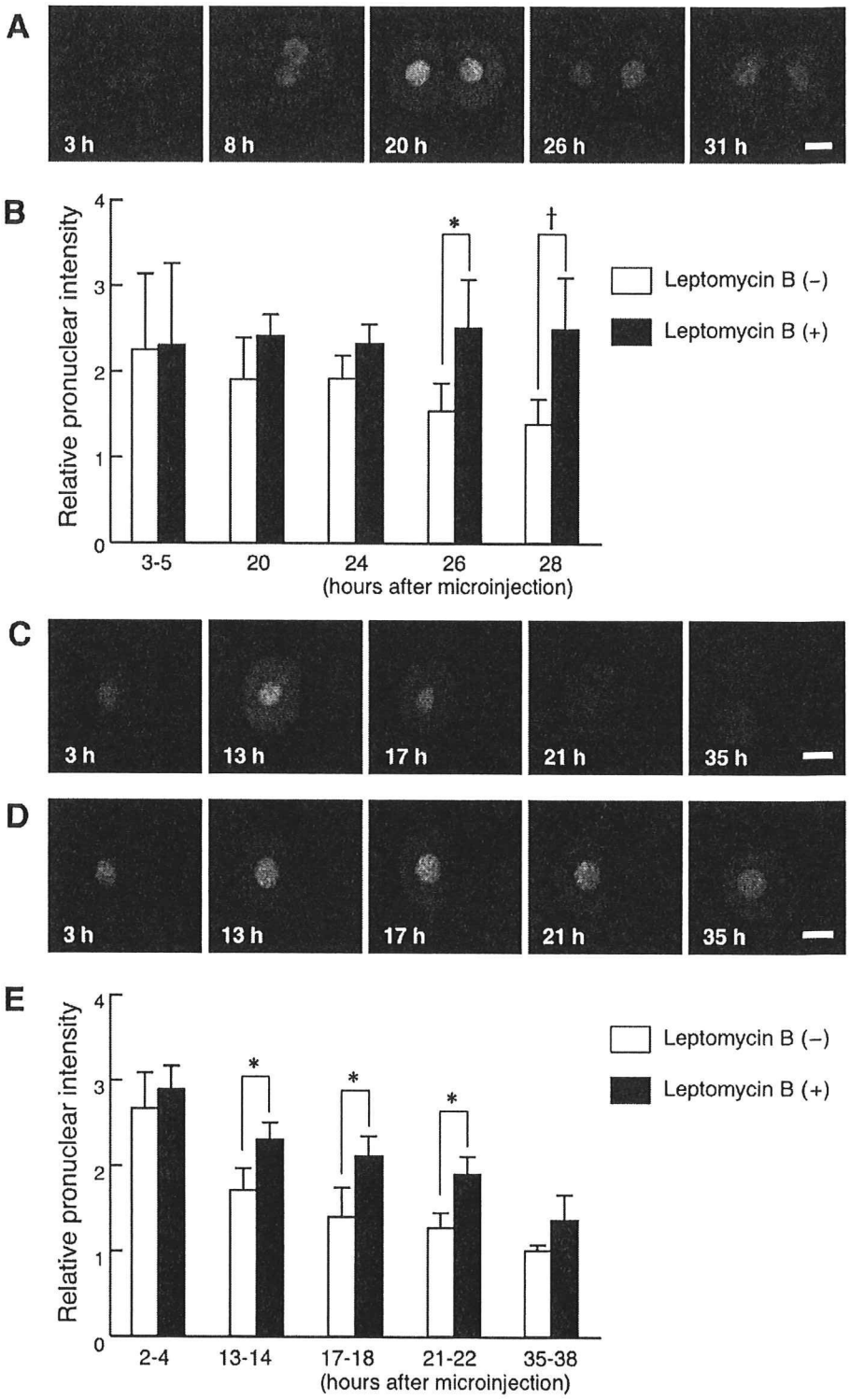


Fig. 4. Effects of leptomycin B on the dynamics of EGFP-Dnmt1s localization. (A) *In vitro* transcripts for EGFP-Dnmt1s were microinjected into one-cell embryos. Embryos were then cultured in the presence of leptomycin B. Fluorescent images were serially obtained by confocal microscopy. Time is in hours after mRNA injection. Scale bars indicate 20 μm. (B) Comparison of the relative nuclear intensity of EGFP-Dnmt1s signals after mRNA injection into one-cell embryos in the absence (open columns) and presence (filled columns) of leptomycin B. The columns and bars represent means±S.D. of 4–6 measurements per data point. $*P<0.05$, $\dagger P<0.01$. (C, D) *In vitro* transcripts for EGFP-Dnmt1s were microinjected into one-half of two-cell embryos. Embryos were then cultured in the absence (C) and presence (D) of leptomycin B. Fluorescent images were serially obtained by confocal microscopy. Time is in hours after mRNA injection. Scale bars indicate 20 μm. (E) Comparison of the relative nuclear intensity of EGFP-Dnmt1s signals after mRNA injection into one-half of two-cell embryos in the absence (open columns) and presence (filled columns) of leptomycin B. The columns and bars represent means±S.D. of 4–6 measurements per data point. $*P<0.005$.

detected around the mitotic chromosomes, although the signals did not completely coincide with the chromosomes (Fig. 2M).

*Nuclear-cytoplasmic shuttling of GFP-Dnmt1s in early preimplantation embryos*

To confirm the dynamics of nuclear Dnmt1s localization and clarify the underlying mechanism, we constructed plasmids encoding fusion proteins of EGFP with full-length Dnmt1s or its mutants (Fig. 3A), and injected their *in vitro* transcripts into early stage embryos. When EGFP-Dnmt1s mRNA was injected into ~200 one-cell embryos 24–26 h after hCG injection, 36 embryos showed EGFP signals in their pronuclei 1–2 h after injection and 11 embryos reached the two-cell stage with nuclear EGFP signals. Disappearance of EGFP-Dnmt1s from the pronuclei at PN5 could be verified in 8 of the 11 embryos (Fig. 3B). At the two-cell stage, EGFP signals were again localized to the nucleus within several hours after the first

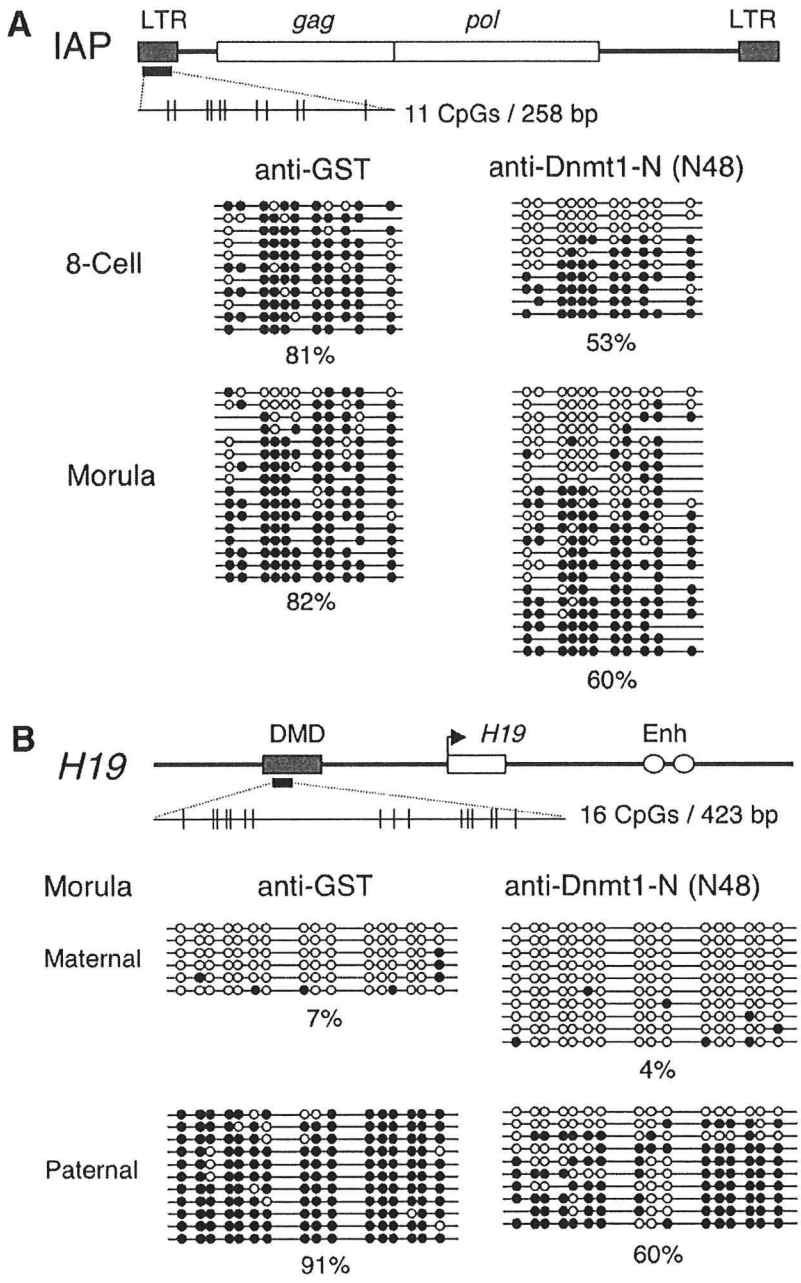


Fig. 5. Effects of antibody microinjection on DNA methylation states in preimplantation embryos. (A) Bisulfite sequencing profiles of the LTR of IAP in antibody-injected embryos at the eight-cell and morula stages. (B) Bisulfite sequencing profiles of the DMD of the paternal *H19* allele in antibody-injected embryos at the morula stage. Open and filled circles represent unmethylated and methylated CpGs, respectively. Each line corresponds to an individual DNA strand. The overall percentage of methylated CpGs is shown below each group of clones.

cleavage, but had mostly disappeared from the nucleus around the G2 phase (Fig. 3B), mimicking the behavior of Dnmt1s-immunoreactivity in embryos at the same stage. When EGFP-Dnmt1o mRNA was injected into one-cell embryos, EGFP-Dnmt1o protein was also localized to the nucleus as in case of EGFP-Dnmt1s (Fig. 3C). In contrast, EGFP-fusion protein with the N-terminal region containing putative nuclear localization signals (amino acids 112–263) resulted in retention of EGFP signals in the nucleus (Fig. 3D). These results indicate that the disappearance of Dnmt1 from the (pro)nucleus is not due to the presence of EGFP and does not require the Dnmt1s-specific N-terminal region.

To test whether the decrease in nuclear EGFP signals was attributable to active nuclear export, embryos were injected with EGFP-Dnmt1s mRNA at the one-cell stage and then treated with leptomycin B, an inhibitor of CRM1/exportin-mediated nuclear export. EGFP signals were retained in the nucleus with high intensity in leptomycin B-treated embryos (Figs. 4A, B). EGFP-Dnmt1s mRNA was also injected into one-half of two-cell embryos 1–4 h after the first cleavage. Among ~220 embryos injected, 22 expressed EGFP-Dnmt1s protein in the injected half. In all seven embryos that grew to the four-cell stage within 36 h after the first cleavage, nuclear EGFP-Dnm1s signals were largely suppressed during the G2 phase, whereas cytoplasmic EGFP signals were sustained (Fig. 4C). In the presence of leptomycin B, however, EGFP signals were retained in the nucleus with high intensity (Fig. 4D). These results indicate that the decrease in nuclear EGFP-Dnmt1s

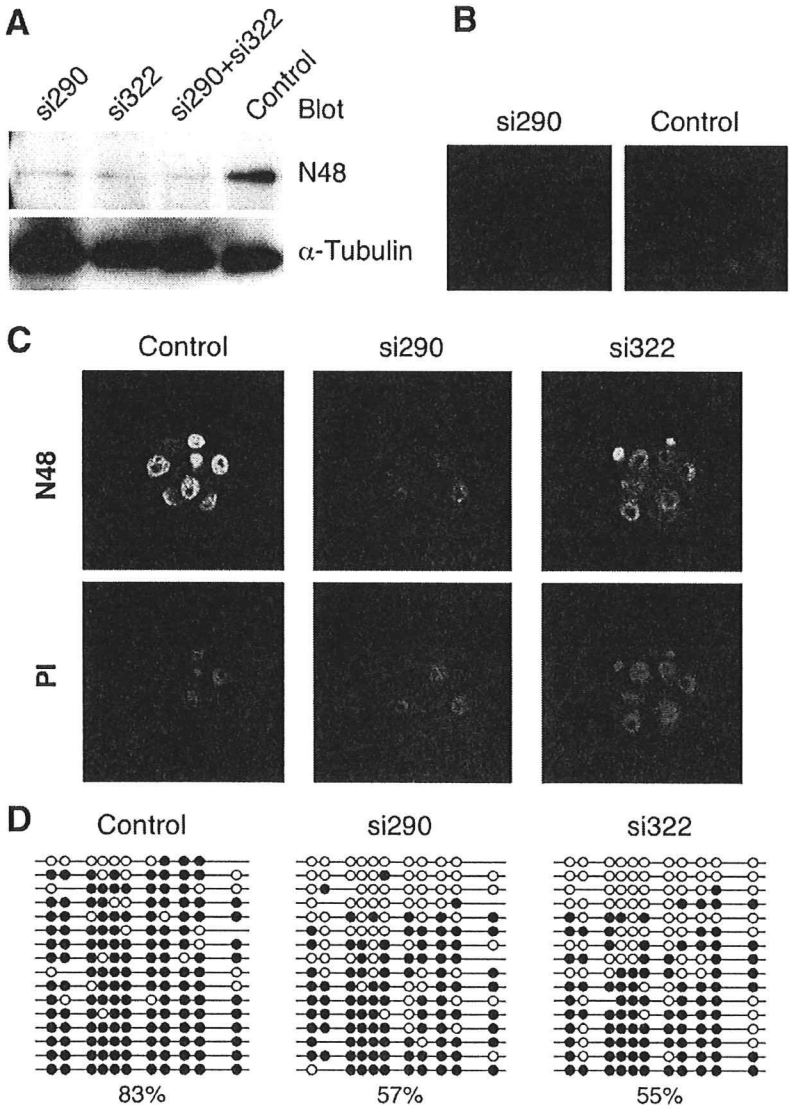


Fig. 6. Effects of Dnmt1-targeted siRNA microinjection on DNA methylation states in preimplantation embryos. (A, B) Efficient downregulation of Dnmt1s protein by siRNA was verified in NIH 3T3 cells by Western blotting (A) and immunostaining (B) with N48 antibody. (C) Immunostaining analysis of 8–16 cell embryos injected with control and Dnmt1 siRNA, probed with the N48 antibody. DNA was counterstained with PI. Dnmt1 expression is effectively knocked-down in Dnmt1 siRNA-injected embryos. (D) Bisulfite sequencing profiles of the IAP LTRs in siRNA-injected embryos at the morula stage. Open and filled circles represent unmethylated and methylated CpGs, respectively. Each line corresponds to an individual DNA strand. The overall percentage of methylated CpGs is shown below each group of clones.

during the G2 phase is attributable to CRM1/exportin-dependent nuclear export.

*Microinjection of anti-Dnmt1 antibody affects DNA methylation patterns*

To examine whether Dnmt1s present in preimplantation embryos is responsible for the maintenance of DNA methylation during this stage, we evaluated genomic methylation patterns using two different approaches. First, we performed ICSI with co-injection of N48, expecting that it might function as a Dnmt1s-specific neutralizing antibody. In control embryos injected with anti-GST antibody, the long terminal repeats (LTR) of IAPs were highly methylated as revealed by bisulfite sequencing at the eight-cell and morula stages (81% and 82%, respectively) (Fig. 5A). Injection with N48 antibody resulted in a significant decrease in DNA methylation of IAPs at the morula stage (60%, $P<0.05$) (Fig. 5A). Similar phenomenon was observed at the 8-cell stage, although it was not statistically significant (53%, $P=0.064$) (Fig. 5A). Notably, some IAP sequences showed complete or nearly-complete demethylation in N48-injected embryos, which was consistent with the failure of DNA methylation maintenance (Fig. 5A). We also analyzed the effect of N48 injection on the methylation state of the paternally imprinted *H19* gene. To determine the parental origins of alleles, we injected sperm from *M. m. castaneus* males into oocytes from ICR females with N48 or control anti-GST antibodies. In embryos injected with control antibody, the differentially methylated domain (DMD) of the *H19* gene of the paternal allele was highly methylated at the morula stage (91%), whereas that of the maternal allele was mostly demethylated (7%) (Fig. 5B). In N48-injected embryos, the percentage of DNA methylation in this region of the paternal allele was significantly decreased (60%, $P<0.01$), whereas that of the maternal allele was similarly demethylated (4%) (Fig. 5B). These results indicate the methylated CpGs dinucleotides in the IAP and *H19* gene loci to be decreased by microinjection of anti-Dnmt1s antibody.

*Dnmt1-targeted siRNA affects DNA methylation patterns*

To further investigate the role of Dnmt1s in maintenance methylation, we adopted RNAi-mediated knock-down experiments because Dnmt1s, rather than Dnmt1o, is known to be actively transcribed during preimplantation development (Ratnam et al., 2002 and our unpublished data). siRNA was designed to target against Dnmt1s mRNA and tested in NIH 3T3 cells. Western blotting (Fig. 6A) and immunostaining with N48 antibody (Fig. 6B) confirmed the effectiveness of the siRNA. We then injected Dnmt1s siRNA duplexes into fertilized eggs at the pronuclear stage and analyzed their effects on the methylation state of IAPs to test whether the decrease in DNA methylation induced by antibody injection could be reproduced by RNAi-mediated Dnmt1s knock-down. Two independent siRNAs, si290 and si322, against Dnmt1s down-regulated Dnmt1s expression also in preimplantation embryos, as revealed by immunostaining (Fig. 6C). Microinjection of either Dnmt1s siRNA resulted in significant decreases in DNA methylation of IAPs at the morula stages (57% and 55%, $P<0.05$ for si290 and si322, respectively), as compared with that of embryos injected with a control siRNA (83%) (Fig. 6D). As in N48-injected embryos, some IAP sequences demonstrated complete or nearly-complete demethylation (Fig. 6D). Taken together, these results indicate that Dnmt1s synthesized after fertilization is involved in the maintenance methylation of certain repetitive sequences and imprinted genes.

## Discussion

Fertilization initiates epigenetic reprogramming to establish totipotency in the early embryo. Large part of the gametic genome undergoes active or passive DNA demethylation and chromatin remodeling into a zygotic pattern. In contrast, the methylation states of some genomic regions including repetitive sequences and imprinted genes are faithfully maintained during the same period. Failure to identify the enzyme(s) responsible for maintenance DNA methylation in the nucleus of preimplantation embryos, expect for Dnmt1o at the eight-cell stage, has hampered the clarification of mechanisms by which the genomic sequences are selected for demethylation or maintenance methylation and epigenetic reprogramming proceeds precisely.

In the present study, we demonstrated the presence of Dnmt1s protein in the nuclei of preimplantation embryos. This finding is quite contrary to previous literature demonstrating that no Dnmt1s protein is translated from its mRNA during this period. Very low amounts of Dnmt1s relative to cytoplasmic Dnmt1o may have prevented it from detection. Especially, the UPT82 antibody, which can recognize the Dnmt1s-specific N-terminal region, has been reported to detect Dnmt1s in preimplantation embryos when Dnmt1s is forcedly expressed in oocytes (Ratnam et al., 2002), and in 4-,8- and 16-cell embryos that are missing Dnmt1o (Chung et al., 2003). In the later case, loss of Dnmt1o is assumed to cause aberrant expression of Dnmt1s. This apparent discrepancy may be due to differences in sensitivity of antibodies and/or epitope sites to be recognized, which might be protected from recognition by posttranslational modification or complex formation. Indeed, it has been reported that an antibody which recognizes the Dnmt1s-specific N-terminal region could detect Dnmt1s protein in association with mitotic chromatin in somatic cells, while other antibodies could not detect it (Easwaran et al., 2004), indicating the detectability of Dnmt1s may be context-dependent even in the same cells.

Asymmetric distribution of Dnmt1s in the parental genome may be linked to differential reprogramming processes after fertilization. Upon fertilization, the paternal genome undergoes extensive demethylation before the initiation of DNA replication, whereas the maternal genome is protected from this active demethylation and completes the second meiosis. Although the mechanism of active demethylation remains unknown, epigenetic differences between gametes at fertilization are thought to contribute to the establishment of this parental asymmetry (Morgan et al., 2005). The presence of Dnmt1s, together with